Eur. Phys. J. A **44**, 321–354 (2010)
DOI 10.1140/epja/i2010-10964-4

THE EUROPEAN PHYSICAL JOURNAL A

Review

The status of "polarized fusion"

H. Paetz gen. Schieck[a]

Institut für Kernphysik, Universität zu Köln, D-50937 Köln, Germany

Received: 26 October 2009 / Revised: 3 January 2010
Published online: 31 March 2010 – © Società Italiana di Fisica / Springer-Verlag 2010
Communicated by R. Krücken

Abstract. After an introduction into the essentials of nuclear fusion reactions, being considered for future energy production in fusion reactors, different aspects of using "polarized" particles as fuel are discussed. Special emphasis is given to the four-nucleon system and the D+D reactions. The status of the theory and the experimental data are presented. Predictions for observables in the framework of existing theoretical approaches are given. The necessity of carrying out direct spin-correlated cross-section measurements is accentuated. Details of a future experiment are proposed.

Contents

[a] e-mail: schieck@ikp.uni-koeln.de

1 Introduction

Increasing energy demand in view of limited supply, as well as environmental concerns leading to increased emphasis on renewable energy sources such as solar or wind energy also will focus public and scientific interest again on nuclear power, and especially fusion energy. With the decision to build ITER (low-density magnetic confinement) and also continuing research on (high-density) inertial-confinement fusion, prospects of fusion energy may have entered a new era. The idea of "polarized fusion", developed already long ago ([1,2], and for more recent developments see [3]), which undoubtedly offers a number of advantages over unpolarized fusion, will gain new impetus. The main features are:

– Neutron management: replacement or reduction of neutron-producing reactions in favor of charged-particle reactions.
– Handling of the emission direction of reaction products.
– Increase of the reaction rate.

Part of these improvements may lead to lower ignition limits and to more economical running conditions of a fusion reactor due to less radiation damage and activation to structures and especially the blanket, necessary to convert the neutron energy to heat, or may lead to concepts of a much simpler and longer-lasting blanket. At the

same time its realization will meet additional difficulties for which solutions have to be studied. Some of these are:

- Preparation of the polarized fuel, either in the form of intense beams of polarized ^{3}H, D, or ^{3}He atoms or as pellets filled with polarized liquid or solid.
- Injection of the polarized fuel.
- Depolarization during injection or during ignition.

As an example of a recent effort to address some of these questions we cite ref. [4]. All these questions cannot be discussed here in detail, as they would require intense and specialized research. Instead some unsolved problems with the basic fusion reactions will be addressed. They have to do with the fact that, in order to be able to judge the effects of polarization on fusion energy, experimental polarization data of the very low-energy fusion reactions with sufficiently high precision such as spin-correlated cross-sections are necessary. However, they have not been measured. Existing reaction analyses and predictions for polarized fusion relied on existing world data sets of other (simpler) data. On the other hand, sufficiently microscopic and therefore realistic theoretical predictions (such as for the three-nucleon system) do not yet exist for the four- and five-nucleon systems at the required low energies. It is also not clear whether the recently discussed electron-screening enhancement ([5] and references therein) of the very-low-energy cross-sections has any bearing on polarized fusion.

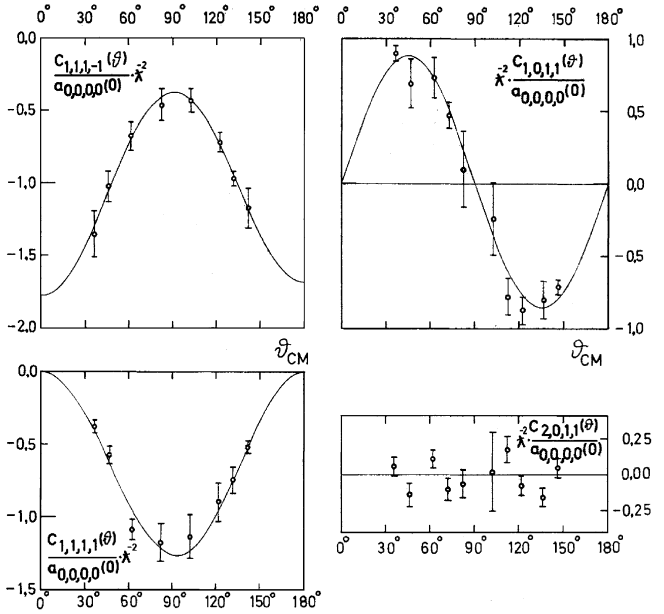

Fig. 1. Spin-correlation measurement of the $^3\vec{\mathrm{H}}\mathrm{e}(\vec{d},p)^4\mathrm{He}$ reaction at $E_d = 430\,\mathrm{keV}$ [6,7]. (From [6] by permission of Birkhäuser Verlag, Basel.)

2 Fusion reactions for energy production

Fusion reactions for energy production are limited to light nuclei, basically the isotopes of hydrogen and helium. At the relevant low energies the Coulomb barrier determines the reaction rates. Besides, only reactions with high positive Q-value can be used. Thus mainly four- and five-nucleon reactions are being considered. The relevant quantities are the integrated (or total) cross-section σ, the reaction coefficient (or reaction parameter) $\langle\sigma v\rangle$ and the (relative) power density P_f.

2.1 Five-nucleon fusion reactions

The important reactions to be discussed here are:

- $d + {}^3\mathrm{H} \rightarrow n + {}^4\mathrm{He} + 17.58\,\mathrm{MeV}$,
- $d + {}^3\mathrm{He} \rightarrow p + {}^4\mathrm{He} + 18.34\,\mathrm{MeV}$.

The two mirror reactions have some very pronounced features:

- At the low energies discussed here both proceed via strong S-wave resonances (at deuteron laboratory energies of 107 keV for $^3\mathrm{H}(d,n)^4\mathrm{He}$, and 430 keV for $^3\mathrm{He}(d,p)^4\mathrm{He}$, respectively). These resonant states are quite pure $J^\pi = 3/2^+$ states with possibly very little admixture of a $J^\pi = 1/2^+$ S-wave and/or higher wave contributions. This has been a long-time point of discussion, mainly because of the reactions being very good absolute tensor-polarization analyzers, provided they proceed only through the S-wave $J^\pi = 3/2^+$ state. Experimental evidence shows that other contributions are small (of the order of a few %). An example of the $^3\mathrm{He}(d,p)^4\mathrm{He}$ reaction on resonance is an early spin-correlation measurement [6,7] supporting this assumption, see fig. 1. For a recent discussion see, *e.g.*, refs. [8,9]. The results for the mirror reaction $^3\mathrm{H}(d,n)^4\mathrm{He}$ are similar. Because, for practical purposes, the transitions essentially go through *one* transition-matrix element, predictions about the behavior of cross-sections and polarization observables can be made quite reliably. The magnitude of the cross-sections is an experimentally determined quantity. For plots of the excitation functions of the cross-sections see sect. 3.
- They have very high cross-sections at resonance. This makes especially the $^3\mathrm{H}(d,n)^4\mathrm{He}$ reaction the first choice for fusion energy due to its highest reaction yield and energy density at the lowest temperature of the plasma. The 3.5 MeV α particles produced will be useful for heating the plasma. The resulting high-energy (14.1 MeV) neutrons, however, which must be captured in a "blanket" wall, create problems, *e.g.* with material modifications. These problems, finally, lead to economic ones. Therefore, the neutronless mirror reaction $^3\mathrm{He}(d,p)^4\mathrm{He}$, appears ideal, except for the higher temperature needed for ignition. A reactor, using this latter reaction, would in addition not be completely neutronless due to the $^2\mathrm{H}(d,n)^3\mathrm{He}$ reaction occuring simultaneously.
- Polarizing the particles in the initial channel in a stretched configuration (spin 3/2) offers the interesting possibility of increasing the fusion yield, *i.e.* lowering

the breakeven limit of a reactor. The cross-section for unpolarized particles is an incoherent mixture of transitions from the $J^\pi = 3/2^+$ and from the $J^\pi = 1/2^+$ state with their statistical weights. Thus the transition is excited with a probability $g = \frac{2J+1}{(2a+1)(2b+1)}$ where J is the spin of the "compound state", a and b the spins of the colliding incident particles. Here the high cross-section transition through the $3/2^+$ state has $g = 2/3$. When describing all possibilities, more precisely, the formation of the $J = 3/2$ state is governed by Clebsch-Gordan coefficients of the coupling of the spin states of the two incident particles colliding and forming the coupled state J:

$$(I_1 I_2 m_1 m_2 | JM).$$

For deuterium ($J = 1$) on tritium (or ^{3}He, $J = 1/2$), thus the CG coefficients $(1\frac{1}{2} m_d m_t | \frac{3}{2} M)$ have to be evaluated. If we denote the three possible spin substates of the deuteron, as referred to a quantization axis (*e.g.*, a magnetic field) as +, 0, and − and the occupation numbers of these substates by their amplitudes a, b, and c as $|a|^2$, $|b|^2$, and $|c|^2$, likewise for tritium (up and down substates + and − with amplitudes d and e) as $|d|^2$ and $|e|^2$, we get the contributions of all spin channels to the cross-section σ, compared to the cross-section σ_{max} in the fully aligned case:

$$\sigma = \left[|a|^2|d|^2 + |c|^2|e|^2 + \frac{2}{3}|b|^2 + \frac{1}{3}(|a|^2|e|^2 + |c|^2|d|^2) \right] \sigma_{max}.$$

Thus, a transition prepared in the pure $J = 3/2$, $M = +3/2$ configuration (alignment along a field B, both beams fully polarized: $|a|^2 = |d|^2 = 1$, all others = 0, equally for a full alignment opposite to the direction of field B: $J = 3/2$, $M = -3/2$, $|c|^2 = |e|^2 = 1$) would be ideally enhanced by a factor 1.5. However, if only one sort of fuel nuclei were fully polarized (*e.g.*, $|a|^2 = 1$, all others = 0), no enhancement over the random (unpolarized) case would occur.
All experimental evidence [6–10], showing small, but non-zero contributions from the other entrance channel S-wave $J = 1/2$ transition as well as from higher partial waves, makes this yield enhancement factor a realistic option. Detailed discussions about the spin structure, its connection to polarization observables and underlying partial-wave amplitudes can be found in refs. [11,12].

2.2 Four-nucleon reactions

Here the relevant re-arrangement fusion reactions are:

- $d + d \rightarrow n + {}^3\mathrm{He} + 3.268\,\mathrm{MeV}$,
- $d + d \rightarrow p + {}^3\mathrm{H} + 4.033\,\mathrm{MeV}$.

Figure 2 shows typical charged-particle spectra at two angles of both DD reactions at $E_d = 28\,\mathrm{keV}$. They were obtained with thin solid-state detectors protected from electrons and elastically scattered deuterons by thin foils and using a thin CD_2 solid target [13].

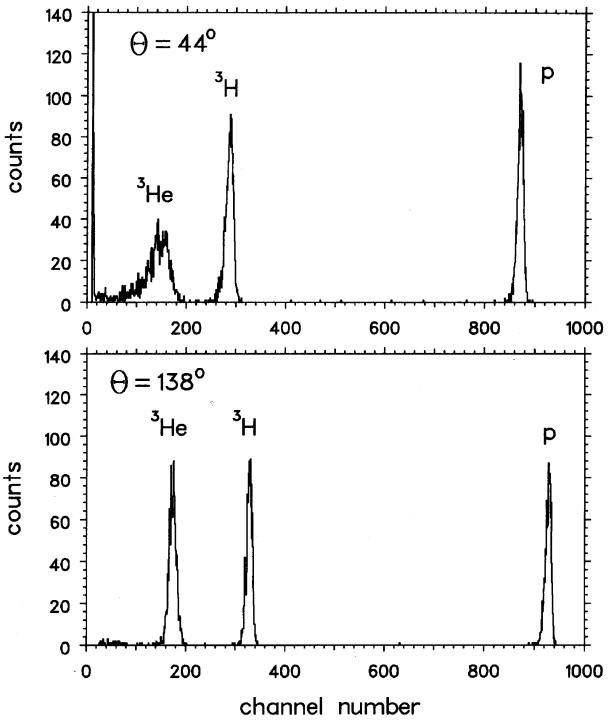

Fig. 2. Typical low-energy charged-particle spectra of DD reactions. (From ref. [13] by permission of Springer-Verlag, Wien.)

2.3 Other reactions

Other possible fusion reactions, but with orders of magnitude smaller power densities at the relevant temperatures, are $p + {}^6\mathrm{Li}$, $p + {}^{11}\mathrm{B}$, ${}^3\mathrm{He} + {}^3\mathrm{He}$, and $p + {}^9\mathrm{Be}$. Reactions such as $n + {}^6\mathrm{Li} \rightarrow {}^4\mathrm{He} + \mathrm{T} + 4.8\,\mathrm{MeV}$ and $n + {}^7\mathrm{Li} \rightarrow {}^4\mathrm{He} + \mathrm{T} + n - 2.47\,\mathrm{MeV}$ have to be considered in order to complete the fuel cycle by breeding ${}^3\mathrm{H}$ (T, tritium) which does not occur naturally. Similar considerations apply to ${}^3\mathrm{He}$ (which is abundant only on the Moon), whereas deuterium is abundant in water on Earth (1 part in 6500).

3 Fusion basics

In this section a few quantities relevant for fusion at low energies will be introduced. These are the basic cross-sections, the reaction parameter which determines the reaction rates in a thermonuclear reactor, and the power density which depends also on the reaction-particle densities.

3.1 Nuclear cross-sections

The basic cross-sections of the relevant nuclear low-energy reactions are shown in fig. 3. The resonant behaviour of

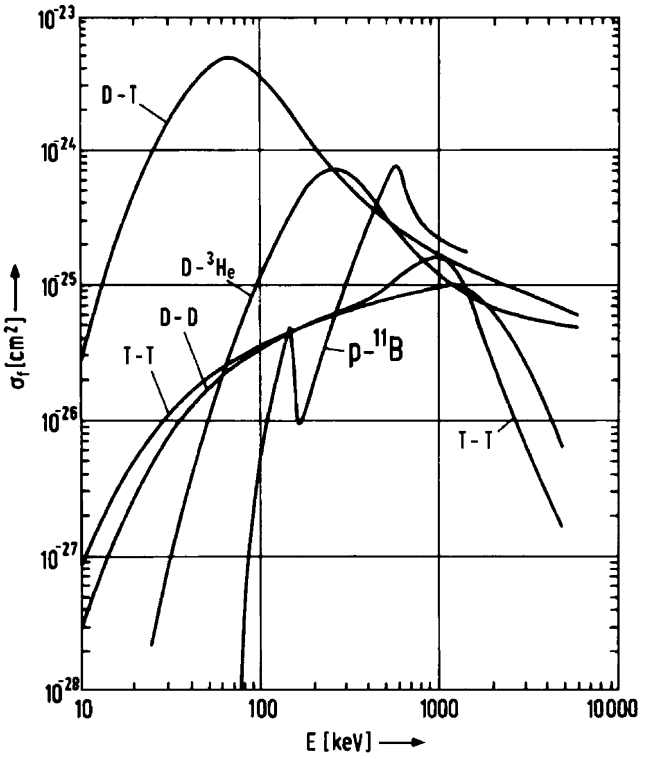

Fig. 3. Integrated cross-sections of fusion reactions as a function of the energy of relative motion (From [14] by permission of Springer-Verlag, Heidelberg.)

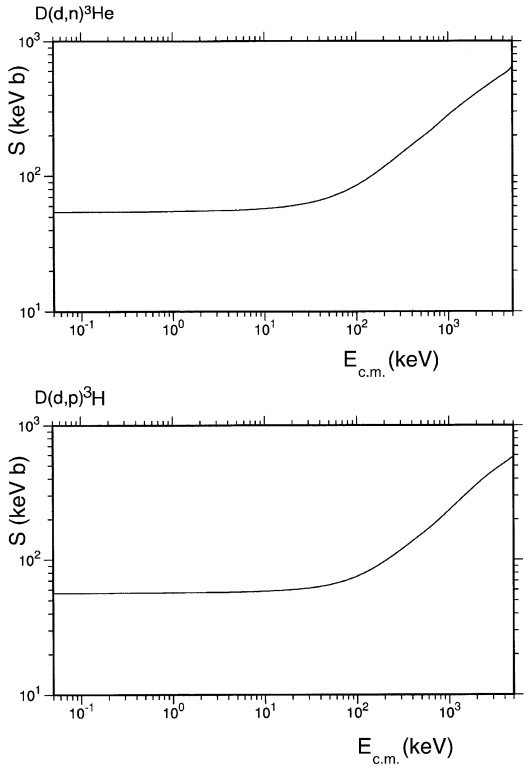

Fig. 4. Astrophysical S-factors showing the non-resonant behavior of DD reactions. Deviations at higher energies are mainly caused by P and D waves.

the five-nucleon reactions is clearly visible whereas other reactions such as the D+D reactions appear non-resonant. It is also evident how the cross-section towards lower energies is entirely dominated by the Coulomb penetrability. In order to separate the influence of the Coulomb penetrability from the nuclear-reaction part it is customary to introduce the astrophysical S-factor $S(E)$ which is defined, using the Sommerfeld parameter with Z_1, Z_2 the charge numbers and μ the reduced mass of the entrance channel particles

$$\eta_S = \frac{Z_1 Z_2 e^2}{\hbar v} = Z_1 Z_2 \left(\frac{e^2}{\hbar c}\right)\frac{c}{v} = Z_1 Z_2 \frac{\alpha}{\beta} = \sqrt{\frac{\mu}{2E_{c.m.}}}\frac{Z_1 Z_2 e^2}{\hbar}.$$

Numerically $\eta_S = 0.1574 \cdot Z_1 Z_2 \sqrt{\frac{A_{red}(u)}{E_{c.m.}\,(\mathrm{MeV})}}$ with A_{red} the reduced mass number.

For S-waves only and assuming a point-Coulomb interaction of the bare nuclei it is

$$S(E_{c.m.}) = \sigma_{tot}(E_{c.m.}) \cdot E_{c.m.} \cdot e^{2\pi\eta_S}.$$

For purely S-wave, non-resonant, reactions in a limited range of low energies the S-factor is smooth and very weakly energy dependent. The S-factors for the DD reactions are shown in fig. 4. The astrophysical S-factors of the $^3\mathrm{H}(d,n)^4\mathrm{He}$ and $^3\mathrm{He}(d,p)^4\mathrm{He}$ reactions in fig. 5 reflect the resonances at deuteron laboratory energies of

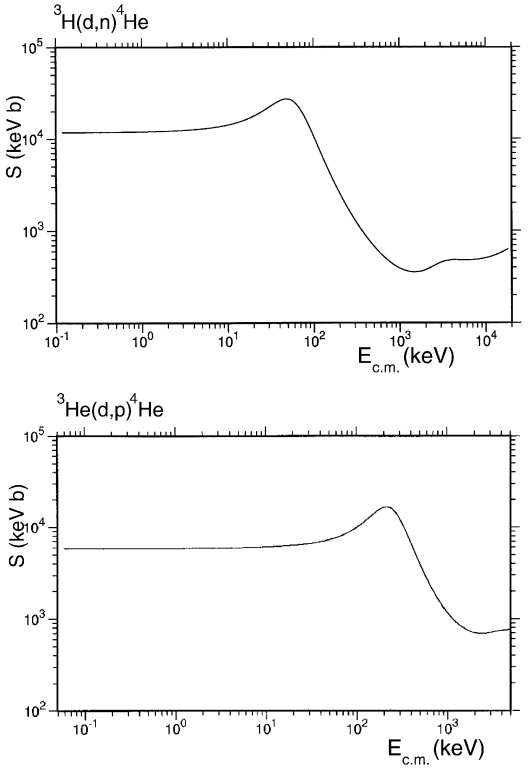

Fig. 5. Astrophysical S-factors, showing the influence of the dominant S-wave, $J = 3/2^+$ resonances in the $^3\mathrm{H}(d,n)^4\mathrm{He}$ and $^3\mathrm{He}(d,p)^4\mathrm{He}$ mirror reactions.

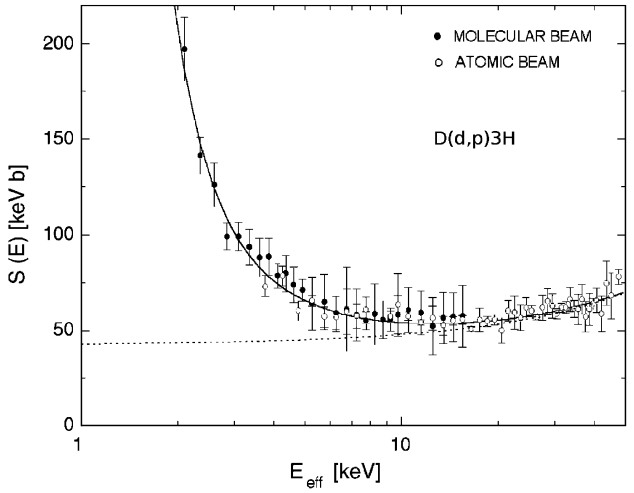

Fig. 6. Astrophysical S-factor of the $^2\mathrm{H}(d,p)^3\mathrm{H}$ reaction with deuterium adsorbed in a solid Ta target, showing the increase of S towards lower energies. (From [15] with kind permission of The European Physical Journal (EPJ).)

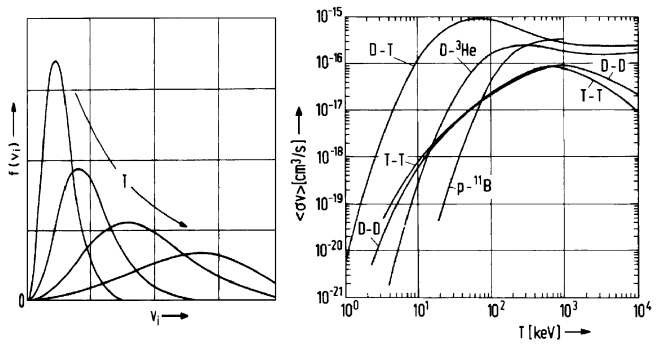

Fig. 7. Maxwell-Boltzmann velocity distributions as functions of velocity v (left) and reaction parameter $\langle\sigma\cdot v\rangle$ as functions of temperature T (right). (From [14] by permission of Springer-Verlag, Heidelberg).

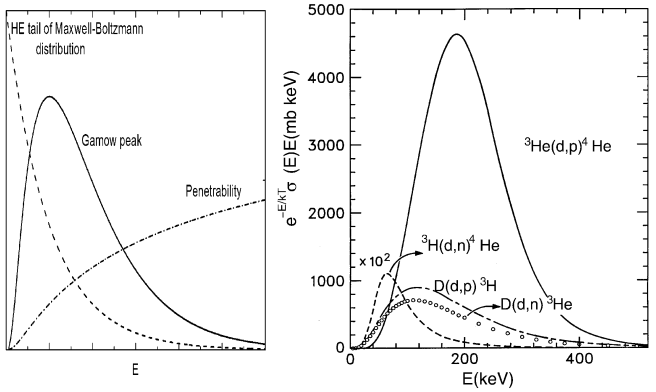

Fig. 8. Assuming that $S(E) \approx$ const, reactions occur in a narrow energy band determined by the Maxwell-Boltzmann distribution together with the penetrability factor (schematically, left). Gamow peaks of the relative reaction rates of the real fusion reactions as a function of energy (right).

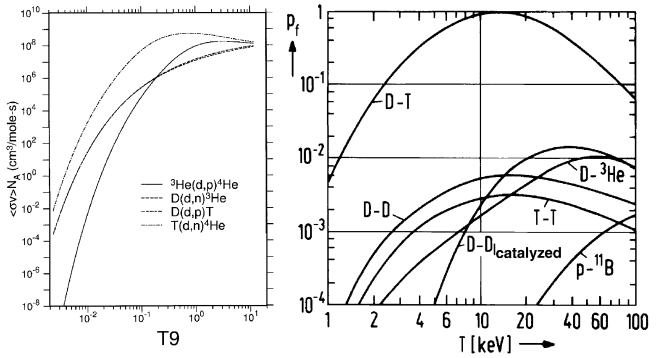

Fig. 9. Relative reaction rates *vs.* temperature $T9$ of deuteron fusion reactions ($T9 \equiv 10^9\,\mathrm{K} \approx 100\,\mathrm{keV}$) (left). Relative power densities as a function of temperature T (normalized to DT at 15 keV) (right). (From [14] by permission of Springer-Verlag, Heidelberg.)

about 107 and 430 keV. At the very low end of the energy scale the effects of screening of the Coulomb potential by the presence of electrons (either in the plasma of gaseous reaction partners or in the metallic environment of solid target materials) will modify (increase) the fusion cross-sections appreciably, see, *e.g.*, [16]. The present status of experiments and theory is, *e.g.*, given in ref. [5]. Here, in fig. 6 an example of the screening effect for the $^2\mathrm{H}(d,p)^3\mathrm{H}$ reaction is shown.

3.2 Thermonuclear reaction rates

Since in a thermonuclear plasma the number of collisions depends on the relative velocity of the particles, and, therefore, on the temperature, the reaction rate depends on the reaction parameter $\langle\sigma\cdot v\rangle$. The average is taken over the Maxwell-Boltzmann velocity distribution shown in fig. 7, together with the reaction parameter. The reaction rates have a distinct maximum in a relatively narrow energy band, the Gamow peak. This can be explained schematically by an interplay of a decreasing high-energy tail of the Maxwell-Boltzmann velocity distribution and the Coulomb penetrability increasing with energy, see fig. 8. The Gamow peaks of real fusion reactions shown in fig. 8 suggest the energy ranges in which fusion reactors have to operate. It is clear that the $^3\mathrm{H}(d,n)^4\mathrm{He}$ reaction is the first choice and the $^3\mathrm{He}(d,p)^4\mathrm{He}$ reaction will be useable only in advanced concepts with higher energies. The finally important quantity is the power density of the fusion plasma which depends on the particle densities of the reaction partners. Figure 9 shows an example of the power densities of different reactions with assumptions about the particle densities and the temperature.

4 Four-nucleon (4N) system

Since the situation of the five-nucleon systems is relatively clear-cut, whereas the four-nucleon systems have a number of problems in their description, especially in view of "polarized fusion", their theoretical and experimental

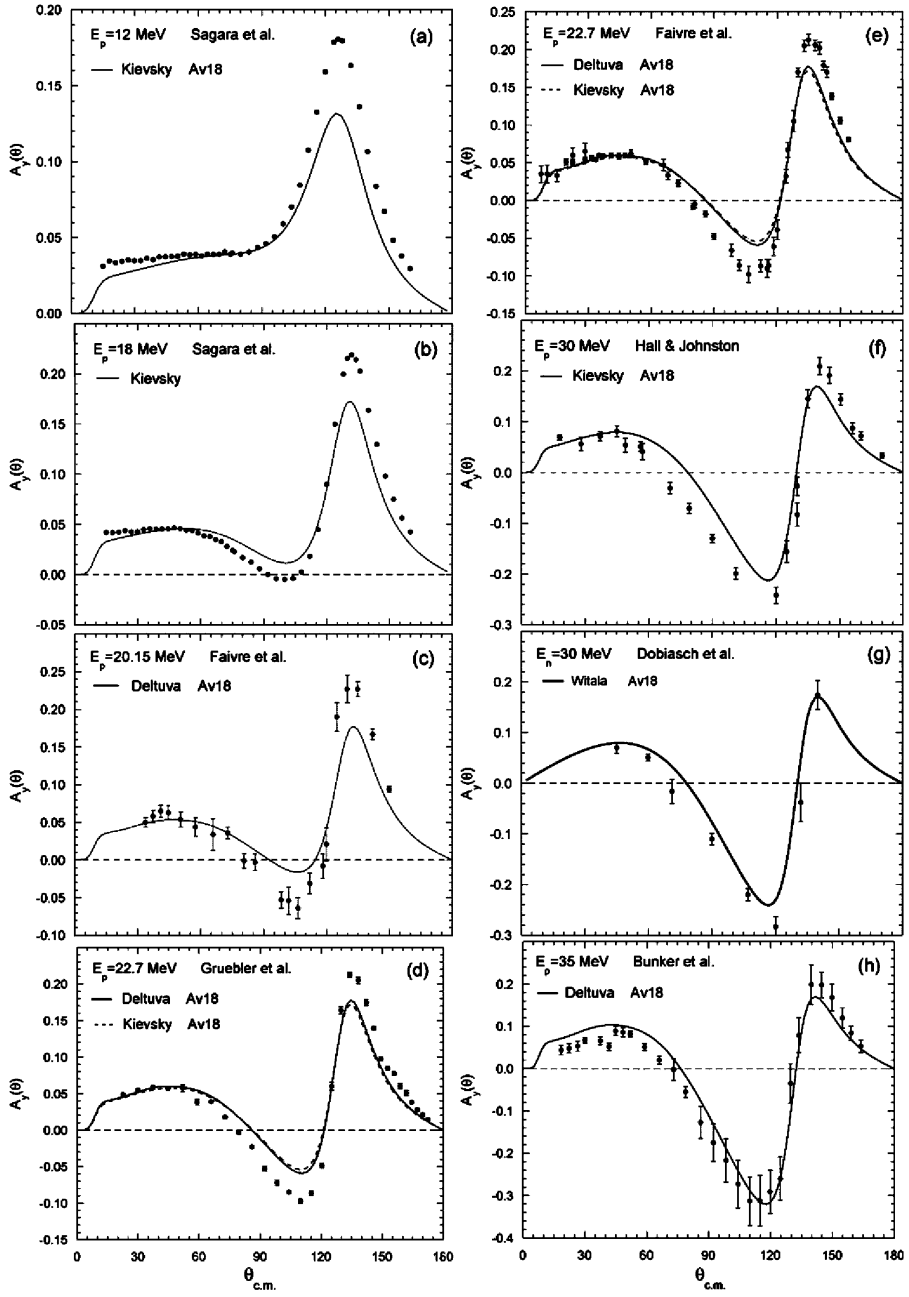

Fig. 10. Systematic discrepancies between A_y measurements and realistic Faddeev predictions (including the Coulomb interaction) at different energies. (From [28] by permission of J. Phys. G, IOP Bristol.)

status will be discussed here in greater detail. In order to understand especially the theoretical situation recourse is taken to a description of the three-nucleon case. The general features of polarized fusion for both systems will be treated together in sect. 5.

4.1 The D+D reactions

Different from the five-nucleon case the reaction mechanism is very complicated (16 complex matrix elements including S, P, and D waves as well as spin-flip transitions from the entrance to the exit channel contribute even at low energies). They are the only reactions with appreciable vector-analyzing power even near 20 keV laboratory energy which cannot be produced by S-waves only.

There is inherent and growing interest in the 4N system for the following reasons:

– It offers itself as testing ground for microscopic (realistic) calculations. Methods of approach have been *Faddeev-Yakubovsky* [17] and *(Refined) Resonating Group Method, RRGM* [18] calculations as well as recent attempts in the framework of effective-field theo-

ries (EFT, chiral perturbation theory χPT to different orders). However, theoretical progress has been slow as compared to the three-nucleon case because of the much more complicated structure of the 4N system and the enormous difficulties connected with an exact solution of the Coulomb problem, especially at low energies.

– Comparisons of experimental results with theoretical predictions show that unsolved discrepancies in the 3N system reappear, even more strongly, in the 4N case (*e.g.*, the well-known A_y puzzle). There is a correlation between 3N and 4N observables (Tjon line, [19]).
– It is the lightest system showing excited states which should be described by theory.
– It offers the possibility of four-nucleon forces though they should be smaller than the three-nucleon force contribution [20,21] (there is no 4N force in NNLO χPT predictions, which —to this order— are parameter free).
– Polarization effects are much larger than in the 3N system even at very low energies (keV region) which is a consequence of the rather strong participation of P and D waves in the entrance channel.
– Besides, in schemes of proposed fusion-reactor designs the very low-energy D+D reactions play a role in astrophysics in connection with the big-bang nucleosynthesis, see *e.g.* [22].

4.2 Comparison with the 3N system and unresolved discrepancies

Some of these topics will be explained by the following examples. In order to be able to assess the status of the theory it is necessary to consider the 3N system though the latter is of no importance to the fusion-energy field. The status of the low-energy theory may be summarized as follows. "Classical" numerically-exact Faddeev calculations use realistic nucleon-nucleon potentials (Nijmegen, CD Bonn, Argonne 18 etc.) as input for the *nd* system and, in addition, three-nucleon forces such as the (modified) Tucson-Melbourne and the Urbana IX three-nucleon forces [23]. Recently, the inclusion of the Coulomb force allows the description of the *dp* system as well, see, *e.g.*, [24, 25]. Another three-nucleon force was constructed from an intermediate Δ interaction [25]. Most recently the approach of QCD-based effective-field theory (chiral perturbation theory, χPT) to different orders (now up to NNNLO) [26,27] proved equally successful for most observables. However, a small number of distinct discrepancies remain unsolved in the 3N system, which are explained here:

– *The 3N A_y puzzle:* fig. 10 shows that no realistic calculation reproduces A_y of ^{2}H$(p,p)^2$H. This applies to a large energy range as well as to the ^{2}H$(n,n)^2$H scattering, as shown in fig. 11, and also to iT_{11} of deuteron scattering on ^{1}H. For details, see ref. [28].
– *The space star discrepancy in p+d breakup:* fig. 12 shows the typical disagreement between predictions from different realistic calculations and the data of the symmetric space-star configuration of the ^{2}H$(p,pp)n$ cross-section at energies up to about 20 MeV, see, *e.g.*, [29,30].
– *The 4N-A_y puzzle:* the description of the 4N system is closely connected to the 3N case. Of course, the same NN input has to be used in the Faddeev-Yakubovsky calculations, see also [31]. Also in the χPT approach this connection appears naturally. Due to this and the empirically found correlations between the 3N and 4N systems it is not surprising to find the A_y puzzle also in the 4N system, *e.g.* in the analyzing power of elastic p^3He scattering (see *e.g.* [30,32,33]). Figure 13 illustrates this. It is clear that some piece must be missing in the calculations. Nevertheless, in general there is excellent agreement between data and theory.

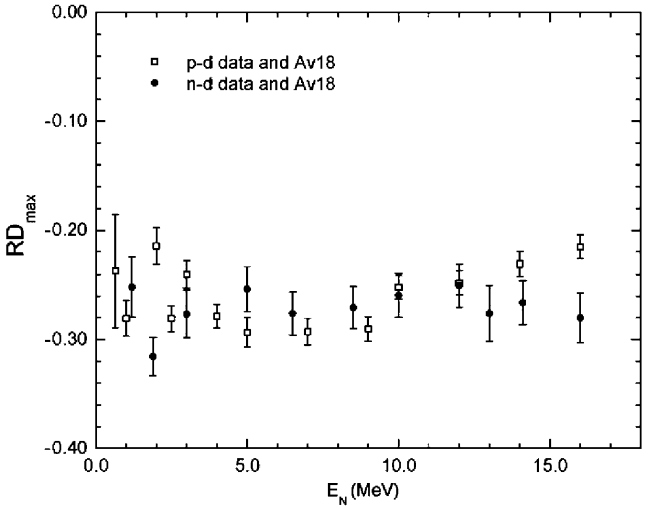

Fig. 11. Relative differences between A_y measurements and realistic Faddeev predictions for *nd* and *pd* (including the Coulomb interaction) elastic scattering as functions of energy. (From [28] by permission of J. Phys. G, IOP Bristol.)

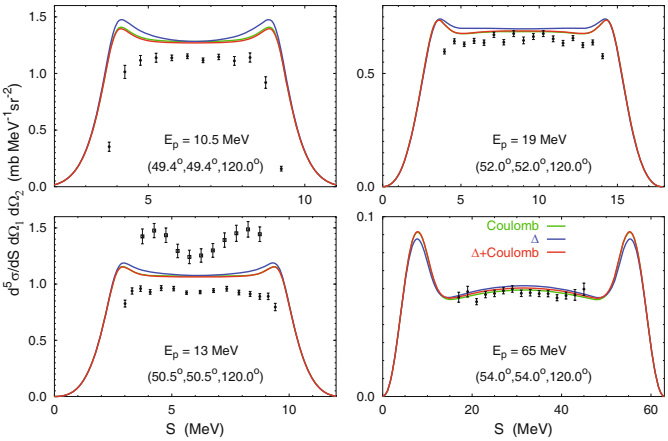

Fig. 12. Disagreement between the cross-sections in the symmetric space-star configuration of the reaction ^{2}H$(p,pp)n$ at several energies and different predictions. (From [30], courtesy of A. Fonseca.) The lower left figure shows in addition the disagreement between the ^{2}H$(p,pp)n$ and the ^{2}H$(n,nn)^1$H data as well as the disagreement of both with *nd* and *pd* calculations.

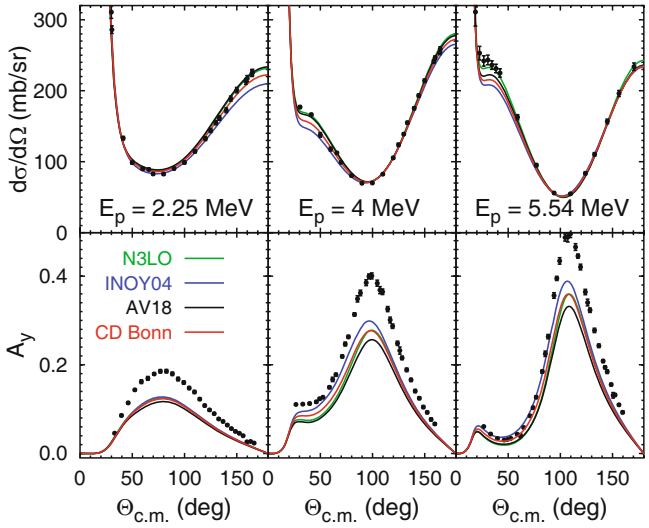

Fig. 13. 4N puzzle: A_y of the ^{3}He$(p,p)^3$He elastic scattering (from [30], courtesy of A. Fonseca).

For the 4N system, however, it is still enormously difficult to make realistic predictions for the astrophysical low-energy range, mainly because of the Coulomb problem which requires huge computing resources [34,35]. However, attempts to provide predictions around 100 keV deuteron energies will be forthcoming [36]. For higher energies, *i.e.* in the MeV range, the present status of the calculations is shown in fig. 14. Cross-sections and analyzing powers of the DD reactions at 3.5 MeV are compared to different "*ab initio*" calculations including the Coulomb force, also with EFT [25,30,37]. Therefore a number of "less-microscopic" approaches have been taken to make such predictions which, for some observables, give partly good agreement, disagreement for others. This is shown in fig. 15 for a set of very-low-energy analyzing-power data taken at Köln [13] which are typical for the DD reactions with relatively large P-wave contribution even at 28 keV. Similar data in this range were published, partly in numerical form, by other groups: Petitjean *et al.* [38], Paetz gen. Schieck *et al.* [39], both at 460 keV, Jeltsch *et al.* at 150, 230, and 340 keV [40], Pfaff at 80, 120, 160, 180, 200, 260, 330, 390, 460, and 1000 keV [41], Tagishi *et al.* at 30, 50, 70, and 90 keV [42], and Fletcher *et al.* at 25, 40, 60, and 80 keV [43]. A survey of the data situation up to 1988 is given in [44].

5 "Polarized" fusion

There are several possible advantages which offer themselves when using polarized particles as fuel in fusion plasmas.

5.1 Yield enhancement of the main reaction

In the ^{3}He$(d,p)^4$He and ^{3}H$(d,n)^4$He mirror reactions the rates are entirely dominated by the pure S-wave $J = 3/2^+$ resonance. Using unpolarized "fuel" this resonance channel competes with the $J = 1/2^+$ channel (with almost no yield) according to the relative statistical weights of 4 *vs.* 2. As shown above, by polarizing both components in the stretched $3/2^+$ configuration, the yield ideally will be enhanced by a factor of 1.5. In order to confirm the actual (theoretical) enhancement factor (*i.e.* without depolarizing conditions of a fusion reactor) spin-correlation measurements should be performed. The pertinent formalism for the cross-section of reactions with polarized spin-1/2 on polarized spin-1 particles has been given in ref. [11] where —in Cartesian notation— the $A_{i,i'}$ are analyzing powers and $C_{i,i'}$ spin-correlation coefficients with $i = x, y, z, xx, xy, \ldots$ for the spin-1 beam with polarization p_i and $i' = x, y, z$ for the spin-1/2 target with polarization $q_{i'}$. The superscripts (b) and (t) refer to beam and target observables, respectively. These observables depend on the reaction dynamics and therefore depend on Θ. The Φ-dependence of the differential cross-section for this case, which is a consequence of introducing coordinate systems,

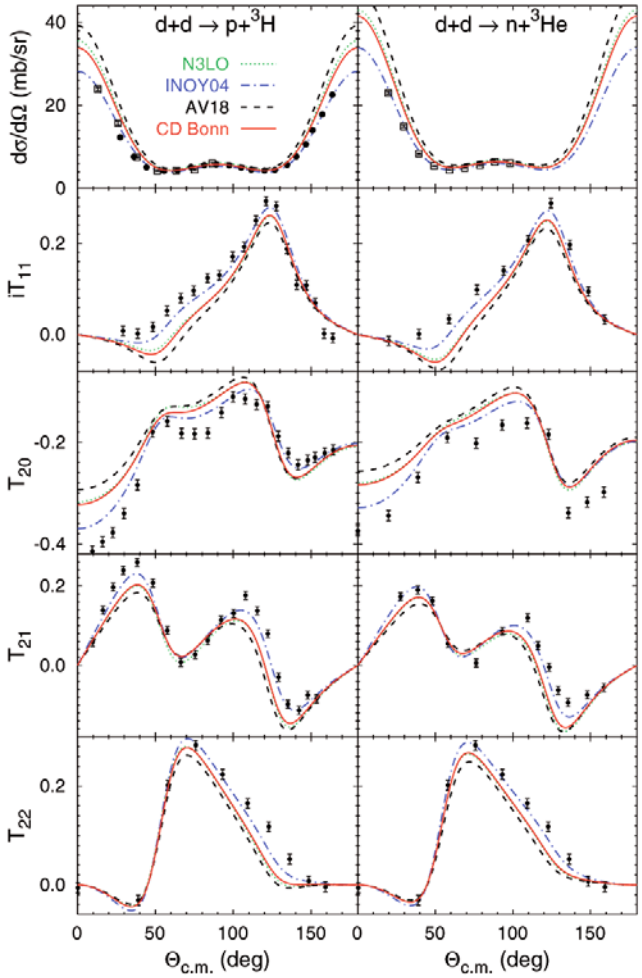

Fig. 14. Present lowest-energy (3 MeV) Faddeev-Yakubovsky and EFT calculations, including the Coulomb force, of observables of the DD reactions. (The figure is reproduced from ref. [37] by permission of APS. Details of the data and calculations are given there.)

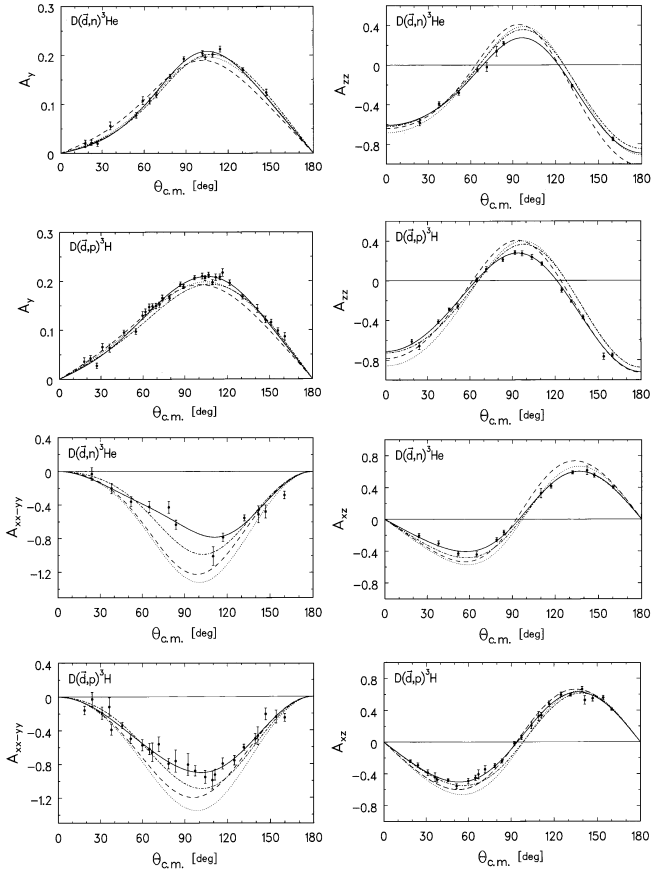

Fig. 15. Vector and tensor analyzing powers of the DD reactions at $E_{lab} = 28\,\mathrm{keV}$ (From ref. [13] by permission of Springer-Verlag, Wien). The lines have the following meaning: Solid: Legendre fit, dashed: R-matrix parametrization [45, 46], dotted and dash-dotted: Köln T-matrix analysis with and without the data shown included [47].

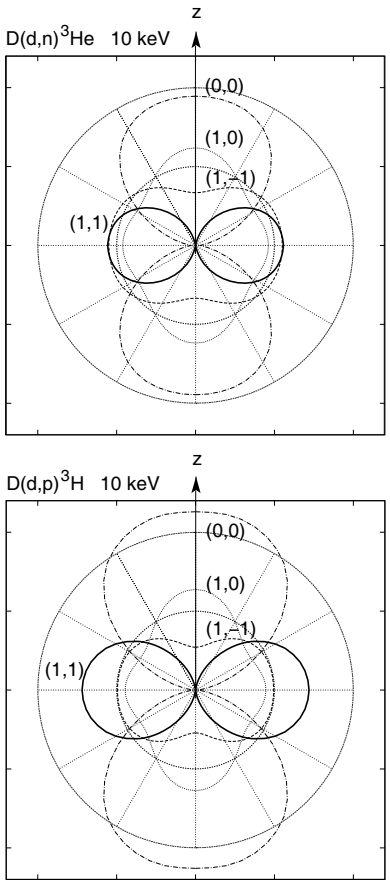

Fig. 16. Emission anisotropies of the spin-dependent partial reaction rates $\langle \sigma_{m,n} \cdot v \rangle$ of the $^2\mathrm{H}(d,p)^3\mathrm{H}$ and $^2\mathrm{H}(d,n)^3\mathrm{He}$ reactions at a plasma temperature corresponding to $kT = 10\,\mathrm{keV}$ and for different deuteron spin orientations, from R-matrix parametrization, calculated from data of ref. [48]. In ref. [48] also calculations for other energies and for cross-sections are given. The averaging was done over the Maxwellian velocity distribution for temperature T. Results for both reactions are shown on the same (relative) scales.

is explicitly discussed in [11] (see also below for the case of spin-1 on spin-1 correlations):

$$
\begin{aligned}
&[\sigma(\Theta,\Phi)]_{\Phi=0} = \\
&\sigma_0(\Theta)\Big\{1 + \frac{3}{2}A_y^{(b)}(\Theta)p_y + A_y^{(t)}q_y \\
&+\frac{1}{2}A_{zz}^{(b)}(\Theta)p_{zz} + \frac{2}{3}A_{xz}^{(b)}(\Theta)p_{xz} + \frac{1}{6}A_{xx-yy}^{(b)}(\Theta)p_{xx-yy} \\
&+\frac{3}{2}[C_{x,x}(\Theta)p_xq_x + C_{y,y}(\Theta)p_yq_y + C_{z,z}(\Theta)p_zq_z \\
&+C_{z,x}(\Theta)p_zq_x + C_{x,z}(\Theta)p_xq_z] \\
&+\frac{2}{3}[C_{xy,x}(\Theta)p_{xy}q_x + C_{yz,x}(\Theta)p_{yz}q_x \\
&+C_{xz,y}(\Theta)p_{xz}q_y + C_{xy,z}(\Theta)p_{xy}q_z + C_{yz,z}(\Theta)p_{yz}q_z] \\
&+\frac{1}{6}C_{xx-yy,y}(\Theta)p_{xx-yy}q_y + \frac{1}{2}C_{zz,y}(\Theta)p_{zz}q_y\Big\}.
\end{aligned}
$$

This expression is overdetermined, which leads to the relation

$$C_{xx,y} + C_{yy,y} + C_{zz,y} = 0.$$

In actual measurements the cross-section formula simplifies appreciably by choosing the direction of the polarization vectors along the x, y, or z axis and when, especially under fusion-reactor conditions, the same polarization symmetry axis for beam and target particles can be assumed. If, *e.g.*, both are aligned along the z-axis, in which case there is no Φ-dependence, then

$$\sigma(\Theta,\Phi) = \sigma_0(\Theta)\left[1 + \frac{1}{3}A_{zz}^{(b)}(\Theta)p_{zz} + \frac{3}{2}C_{z,z}(\Theta)p_zq_z\right].$$

If, in addition, pure vector or tensor polarizations can be produced, as in many sources, a very simple expression results.

5.2 Making use of the anisotropic angular distributions of reaction products from polarized-fusion reactions

Particles from fusion reactions are emitted anisotropically when the incident particles are polarized. This may be

used to direct neutrons in preferred directions where their energy can be optimally used or where their damaging effects may be minimized. Detailed predictions, however, need realistic low-energy calculations, especially for the DD reactions. So far, only one calculation in the framework of the R-matrix parametrization has been published, as shown in fig. 16.

5.3 Suppression of unwanted DD neutrons

Aneutronic fusion has a number of advantages (not the least unimportant *economic* ones) over the use of neutron-producing reactions. At an advanced stage the ^{3}H(d,n) reaction could be replaced by the ^{3}He(d,p) reaction. However, DD neutrons would remain.

It has been suggested by theoretical approaches that DD neutrons could be reduced substantially by polarizing the deuterons, thus forming a quintet ($S=2$) state. The main argument was that quintet states in the entrance channel would require spin-flip transitions which are Pauli-forbidden in first order.

So far the (indirect) experimental evidence does not support this conjecture. A direct spin-correlated cross-section measurement is still lacking, but highly desirable.

5.3.1 Evidence for suppression?

Lacking a direct spin-correlation experiment at very low energies, two indirect approaches have been taken: i) parametrization of world data by a multi-channel R-matrix analysis [18]; ii) Köln parametrization of world data of the ^{2}H$(d,n)^3$He and ^{2}H$(d,p)^3$H reactions by direct T-matrix analysis below 1.5 MeV [47,49–52].

Both approaches allow predictions of any observable of the DD reactions, also of the *quintet suppression factor QSF*, as defined below.

5.3.2 Definition of QSF

In order to quantify the extent to which DD neutrons may be suppressed by polarizing the fusion fuel nuclei the "Quintet Suppression Factor (QSF)" is defined as

$$\mathrm{QSF} = \frac{\sigma_{1,1}}{\sigma_0}$$

with

$$\sigma_0 = \frac{1}{9}\left(\underbrace{2\sigma_{1,1}}_{\text{Quintet}} + \underbrace{4\sigma_{1,0}}_{\text{Triplet}} + \underbrace{\sigma_{0,0}+2\sigma_{1,-1}}_{\text{Singlet}}\right)$$

the total (integrated) cross-section to which the four independent channel-spin cross-sections $\sigma_{1,1}$ (spin quintet configuration), $\sigma_{1,0}$ (spin triplet), $\sigma_{0,0}$, and $\sigma_{1,-1}$ (two spin-singlet terms) contribute with their statistical weights.

In fig. 25 below all results for the QSF from different theoretical predictions, as well as from two data parametrizations for both DD reactions, will be shown and discussed.

6 General reaction formalism

A general reaction formalism is given by the Welton formula [53], originally for uncharged particles only, programmed by [54], see also [55]. The formula shown here was modified to comply with the Madison convention [56]. An extension to treat charged-particle reactions by including explicit Coulomb amplitudes has been performed by P. Heiss [57], and to identical particles, see [58]. FORTRAN computer codes based on these versions were developed: FATSON [54], TUFX [59], and TUFID [58]. Especially for application to the DD reactions these codes were modified into TUFXDD and the fit routine DD [49,51]:

$$\begin{aligned} t_{q\gamma,Q\Gamma} = {} & (2k_{in})^{-2}(i\hat{I})^{1/2} \\ & \cdot \sum \begin{Bmatrix} i & I & s_1 \\ q & Q & t \\ i & I & s_2 \end{Bmatrix} \begin{Bmatrix} i' & I' & s_1' \\ q' & Q' & t' \\ i' & I' & s_2' \end{Bmatrix} \\ & \cdot \begin{Bmatrix} l_1 & s_1 & J_1 \\ l & t & L \\ l_2 & s_2 & J_2 \end{Bmatrix} \begin{Bmatrix} l_1' & s_1' & J_1 \\ l' & t' & L \\ l_2' & s_2' & J_2 \end{Bmatrix} \\ & \cdot (l_1 l_2 00|l0)(l_1' l_2' 00|l'0)(lt0\Lambda|L\Lambda) \\ & \cdot (l't'0\Lambda'|L\Lambda')(qQ\gamma\Gamma|t\Lambda)(q'Q'\gamma'\Gamma'|t'\Lambda') \\ & \cdot T^{J_1^{\pi_1}} T^{J_2^{\pi_2}\,*} D^L_{\Lambda'\Lambda}(\Phi,\Theta,0) \\ & \cdot (\hat{i}'\hat{I}')^{-1/2} \\ & \cdot t_{q'\gamma',Q'\Gamma'}. \end{aligned}$$

By introducing generalized analyzing powers containing, *e.g.*, all angular-momentum algebra the formalism can be simplified. Thus it is obvious that every reaction is completely described by the tensor moments of the exit channel β as functions of the tensor moments of the entrance channel α, usually in a partial-wave expansion:

$$\begin{aligned} t^{\beta}_{k_B q_B, k_b q_b} = {} & \frac{1}{\sigma_p(\vartheta)} \frac{1}{k_\alpha^2} \\ & \cdot \sum_{k_A q_A, k_a q_a, \ell} \underbrace{b^{k_B q_B, k_b q_b}_{k_A q_A, k_a q_a}(\ell, T) \cdot D^{\ell}_{q_A+q_a, q_B+q_b}(\Omega)}_{\text{“generalized analyzing power” } \Xi} \\ & \cdot t^{\alpha}_{k_A q_A, k_a q_a}, \end{aligned}$$

where T stands for bilinear combinations of T-matrix elements. The D are rotation functions, in the simplest cases Legendre functions or polynomials containing the geometry of the reaction. The connection of the generalized analyzing powers and matrix elements is that the Legendre expansion coefficients b contain all information about the reaction via bilinear products of the reaction amplitudes T and appear multiplied by the calculable coefficients B taking care of the angular-momentum algebra (spin coupling etc.):

$$\begin{aligned} & b^{k_B q_B, k_b q_b}_{k_A q_A, k_a q_a}(\ell, T) = \\ & \sum_{i,j} B(k_A, q_A, k_a, q_a, k_B, q_B, k_b, q_b, i, j, \ell) \\ & \cdot \begin{Bmatrix} \mathrm{Re}(T_i T_j^*) \\ i\,\mathrm{Im}(T_i T_j^*) \end{Bmatrix} \quad \text{if } \begin{Bmatrix} \sum k = \text{even} \\ \sum k = \text{odd} \end{Bmatrix}. \end{aligned}$$

Table 1. Matrix elements of the two DD reactions allowed by symmetries, sorted after entrance channel orbital angular momenta and channels spins.

	$S_\alpha = 0$ (Singlet)	$S_\alpha = 1$ (Triplet)	$S_\alpha = 2$ (Quintet)
$\ell_\alpha = 0$	$\alpha_0 = \langle {}^1S_0 \vert 0^+ \vert {}^1S_0\rangle$		$\gamma_1 = \langle {}^5S_2 \vert 2^+ \vert {}^1D_2\rangle$
			$\delta_1 = \langle {}^5S_2 \vert 2^+ \vert {}^3D_2\rangle$
$\ell_\alpha = 1$		$\alpha_{10} = \langle {}^3P_0 \vert 0^- \vert {}^3P_0\rangle$	
		$\beta_{11} = \langle {}^3P_1 \vert 1^- \vert {}^1P_1\rangle$	
		$\alpha_{11} = \langle {}^3P_1 \vert 1^- \vert {}^3P_1\rangle$	
		$\alpha_{12} = \langle {}^3P_2 \vert 2^- \vert {}^3P_2\rangle$	
		$\alpha_3 = \langle {}^3P_2 \vert 2^- \vert {}^3F_2\rangle$	
$\ell_\alpha = 2$	$\alpha_2 = \langle {}^1D_2 \vert 2^+ \vert {}^1D_2\rangle$		$\gamma_2 = \langle {}^5D_0 \vert 0^+ \vert {}^1S_0\rangle$
	$\beta_2 = \langle {}^1D_2 \vert 2^+ \vert {}^3D_2\rangle$		$\gamma_3 = \langle {}^5D_2 \vert 2^+ \vert {}^1D_2\rangle$
			$\delta_2 = \langle {}^5D_1 \vert 1^+ \vert {}^3S_1\rangle$
			$\delta_3 = \langle {}^5D_1 \vert 1^+ \vert {}^3D_1\rangle$
			$\delta_4 = \langle {}^5D_3 \vert 3^+ \vert {}^3D_3\rangle$
			$\delta_5 = \langle {}^5D_2 \vert 2^+ \vert {}^3D_2\rangle$

As an example we note that the differential cross-section is given by the outgoing tensor moment $t^{\beta}_{00,00}$ (outgoing intensity) as a function of $t^{\alpha}_{00,00}$ (incoming intensity).

For the description we use the following definition of the DD T-matrix elements:

$$\boxed{T_{\beta\alpha} = \langle {}^{2S_\alpha+1}\ell_{\alpha J} \vert J^\pi \vert {}^{2S_\beta+1}\ell_{\beta J}\rangle}$$

α: entrance channel; β: exit channel.

For historical reasons the T-matrix elements are named as indicated in table 1.

As an example of a T-matrix element expansion of DD observables we choose the differential cross-section. All states with partial waves up to $\ell_\alpha = 2$ are taken into account. The Legendre polynomial expansion of the (unpolarized) differential cross-section reads

$$\boxed{\frac{\mathrm{d}\sigma}{\mathrm{d}\Omega}(\Theta) = \frac{\lambda^2}{36}\Big[a_0 + a_2 P_2(\cos\Theta) + a_4 P_4(\cos\Theta)\Big]}.$$

Similar expansions can be given for all (polarization) observables. For the differential cross-section we show the expansion coefficients as functions of the 16 DD T-matrix elements, as calculated with the TUFID code [54,58]:

$$\begin{aligned}
a_0 &= |\alpha_0|^2 + 5|\delta_1|^2 + 5|\gamma_1|^2 + |\alpha_{10}|^2 + 3|\alpha_{11}|^2 + 3|\beta_{11}|^2 \\
&\quad +5|\alpha_{12}|^2 + 5|\alpha_2|^2 + 5|\beta_2|^2 + 3|\delta_2|^2 + 3|\delta_3|^2 \\
&\quad +7|\delta_4|^2 + |\gamma_2|^2 + 5|\gamma_3|^2, \\
a_2 &= \frac{3}{2}|\alpha_{11}|^2 - 3|\beta_{11}|^2 + \frac{7}{2}|\alpha_{12}|^2 \\
&\quad +4\,\mathrm{Re}(\alpha_{10}\alpha^*_{12}) + 9\,\mathrm{Re}(\alpha_{11}\alpha^*_{12}) \\
&\quad -2\sqrt{6}\,\mathrm{Re}(\alpha_{10}\alpha^*_3) + 3\sqrt{6}\,\mathrm{Re}(\alpha_{11}\alpha^*_3) - \sqrt{6}\,\mathrm{Re}(\alpha_{12}\alpha^*_3) \\
&\quad +\frac{50}{7}|\alpha_2|^2 + \frac{25}{7}|\beta_2|^2 - \frac{3}{10}|\delta_3|^2 - \frac{4}{21}|\delta_4|^2 - \frac{75}{49}|\gamma_3|^2, \\
a_4 &= \frac{90}{7}|\alpha_2|^2 - \frac{60}{7}|\beta_2|^2 + \frac{180}{49}|\delta_2|^2 - \frac{33}{7}|\delta_4|^2.
\end{aligned}$$

7 Data situation

7.1 Earlier T-matrix-element parametrizations

In a number of publications B.P. Ad'yasevich *et al.* discussed the above formalism, including the connection between (polarization) observables and matrix-element combinations [60,61]. They also considered the necessity of performing a "complete experiment", *i.e.* an experiment in which a sufficient number of observables are measured to determine all matrix elements unambiguously. Due to the lack of data the practical realization of this concept was only partly successful. Also the necessary inclusion of D-waves was not done (see [62] and references therein).

7.2 Köln T-matrix-element fit

- Fit parameters are the "internal" transition matrix elements. S, P, and D waves require 16 complex matrix elements, *i.e.* 31 real parameters. Observables at different energies are "combined" using the Coulomb penetrability for the energy dependence.
- The quantities to be fitted are the Legendre expansion coefficients $b^{k_B q_B, k_b q_b}_{k_A q_A, k_a q_a}$ of all measured data $\sigma_0 \cdot \Xi^{k_B q_B, k_b q_b}_{k_A q_A, k_a q_a}$.
- Fit procedure is a χ^2 minimization with the Levenberg-Marquardt algorithm.
- Results: a) moduli and phases of 16 "internal" matrix elements; b) DD interaction radii r_0.

7.3 Penetrability assumption about matrix elements

The T-matrix fit can be considered to be nearly model independent. The only assumption (common in low-energy nuclear astrophysics) entering the calculation is that the

Table 2. Matrix elements from two Köln T-matrix fits to world low-energy DD reactions dataset.

	^{2}H$(d,n)^3$He	^{2}H$(d,p)^3$H	
$\alpha_0 = \langle {}^1S_0 \vert 0^+ \vert {}^1S_0 \rangle$	3.94 ± 1.56 -129 ± 4	3.44 ± 0.10 95 ± 13	4.26 ± 0.62 -25 ± 13
$\alpha_{10} = \langle {}^3P_0 \vert 0^- \vert {}^3P_0 \rangle$	3.94 ± 0.88 -95 ± 16	3.24 ± 0.72 62 ± 7	2.50 ± 0.22 78 ± 9
$\beta_{11} = \langle {}^3P_1 \vert 1^- \vert {}^1P_1 \rangle$	3.76 ± 0.06 -84 ± 22	4.40 ± 0.06 118 ± 13	4.02 ± 0.42 16 ± 14
$\alpha_{11} = \langle {}^3P_1 \vert 1^- \vert {}^3P_1 \rangle$	8.70 ± 0.26 135 ± 19	7.18 ± 1.32 26 ± 6	7.72 ± 0.66 -38 ± 5
$\alpha_{12} = \langle {}^3P_2 \vert 2^- \vert {}^3P_2 \rangle$	3.28 ± 0.02 132 ± 23	0.72 ± 0.12 -108 ± 11	3.02 ± 0.28 -142 ± 6
$\alpha_2 = \langle {}^1D_2 \vert 2^+ \vert {}^1D_2 \rangle$	9.54 ± 3.54 62 ± 10	5.98 ± 0.08 -38 ± 15	8.58 ± 0.62 -169 ± 15
$\beta_2 = \langle {}^1D_2 \vert 2^+ \vert {}^3D_2 \rangle$	5.36 ± 1.54 -112 ± 13	2.58 ± 0.32 84 ± 16	1.70 ± 0.36 143 ± 13
$\alpha_3 = \langle {}^3P_2 \vert 2^- \vert {}^3F_2 \rangle$	0.80 ± 0.38 27 ± 20	2.84 ± 0.62 35 ± 4	2.90 ± 0.28 -36 ± 7
$\gamma_1 = \langle {}^5S_2 \vert 2^+ \vert {}^1D_2 \rangle$	1.02 ± 0.08 1 ± 24	1.18 ± 0.28 -135 ± 1	1.58 ± 0.04 94 ± 15
$\gamma_2 = \langle {}^5D_0 \vert 0^+ \vert {}^1S_0 \rangle$	8.74 ± 2.60 68 ± 12	11.60 ± 0.36 -87 ± 11	7.60 ± 1.06 120 ± 11
$\gamma_3 = \langle {}^5D_2 \vert 2^+ \vert {}^1D_2 \rangle$	7.26 ± 0.92 159 ± 25	6.44 ± 0.58 80 ± 14	5.38 ± 0.62 -73 ± 14
$\delta_1 = \langle {}^5S_2 \vert 2^+ \vert {}^3D_2 \rangle$	1.52 ± 0.24 80 ± 18	1.84 ± 0.00 -24 ± 13	1.66 ± 0.04 -98 ± 7
$\delta_2 = \langle {}^5D_1 \vert 1^+ \vert {}^3S_1 \rangle$	7.08 ± 2.88 -129 ± 0	1.84 ± 0.60 88 ± 20	5.00 ± 0.34 9 ± 7
$\delta_3 = \langle {}^5D_1 \vert 1^+ \vert {}^3D_1 \rangle$	7.02 ± 3.42 -162 ± 15	12.80 ± 0.04 141 ± 11	3.38 ± 0.50 104 ± 10
$\delta_4 = \langle {}^5D_3 \vert 3^+ \vert {}^3D_3 \rangle$	7.56 ± 2.60 63 ± 14	7.50 ± 0.42 -55 ± 13	5.40 ± 0.36 -106 ± 8
$\delta_5 = \langle {}^5D_2 \vert 2^+ \vert {}^3D_2 \rangle$	2.64 ± 0.92 0 ± 0	1.48 ± 0.38 0 ± 0	2.06 ± 0.24 0 ± 0
Interaction radius (fm) χ^2_{red}	7.4 ± 0.3 3.5	7.3 ± 0.2 11.3	6.6 ± 0.1 21.7

energy dependence is entirely governed by the Coulomb barrier penetrability. The actual T-matrix element is therefore factored into an energy-independent inner matrix element and the penetrability function C. Therefore, we assume

$$T_{\beta\alpha}(E) = C_{\ell_\alpha}(E) \quad \underbrace{\hat{T}_{\beta\alpha}}_{\text{“internal” M.E.}}$$

with $C_{\ell\alpha}(E) = \sqrt{P_{\ell\alpha}(E)\exp[i(\delta_{\ell\alpha}+\phi_{\ell\alpha})]}$ and $P_{\ell\alpha}(E) = \frac{1}{F_{\ell\alpha}(E)^2+G_{\ell\alpha}(E)^2}$; F and G are the Coulomb functions and $\delta_{\ell\alpha} = -\arctan(F_{\ell\alpha}/G_{\ell\alpha})$; $\phi_{\ell_\alpha} = \arg\Gamma(\ell_\alpha+1+i\eta)$.

Figure 17 shows the penetrabilities as functions of energy.

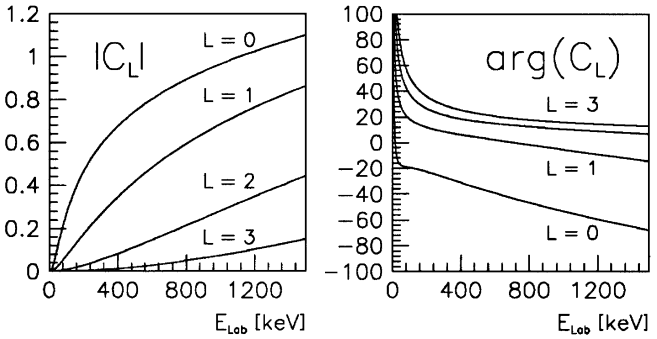

Fig. 17. The penetrability functions $C_{\ell\alpha}$ (with $\ell_\alpha = L$ in the figure) depend on the energy and the orbital angular momenta in the entrance channel α, whereas the internal matrix elements are assumed to be constant over the limited energy range.

7.4 Matrix-element results

Table 2 shows the results of two Köln T-matrix analyses. The first two columns are from ref. [50] for both DD reactions with the deuteron laboratory energy range up to 500 keV. The third column shows the result of an independent fit for ^{2}H$(d,p)^3$H only up to 1.5 MeV [52]. Shown

Table 3. Comparison showing the relative strength of quintet state transitions from different analyses of the $^2\mathrm{H}(d,p)^3\mathrm{H}$ reaction.

	RRGM, Erlangen, Gegner [45]	$A=4$ multi-channel R-matrix fit, Hale, cited by [45]	T-matrix fit, Köln	
			Lemaître *et al.* [50]	Geiger *et al.* [52]
$\frac{\lvert\gamma_1\rvert}{\lvert\alpha_0\rvert}$	0.24	0.92	0.35	0.37
$\frac{\lvert\delta_1\rvert}{\lvert\alpha_0\rvert}$	0.12	0.72	0.48	0.38
$\frac{\lvert\delta_1\rvert}{\lvert\gamma_1\rvert}$	2.0	1.28	1.27	0.95

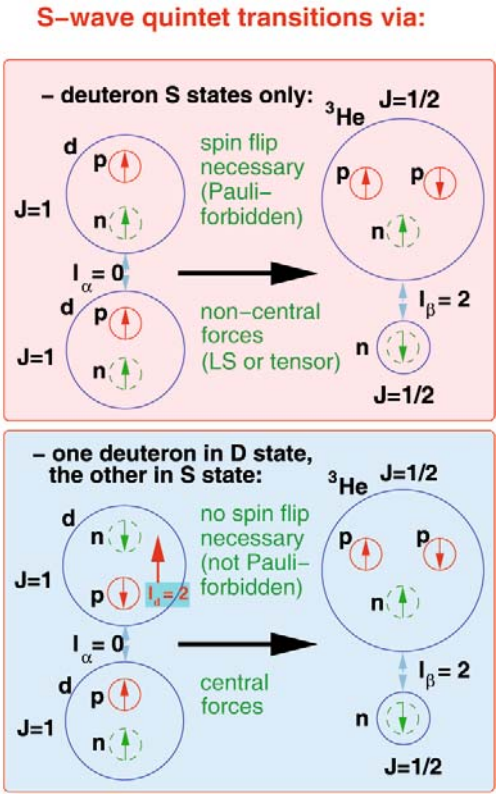

Fig. 18. Without taking into account the deuteron D state, quintet transitions can only occur via spin flip, whereas via the D state no spin flip is necessary. This explains plausibly why quintet transitions may not be strongly suppressed.

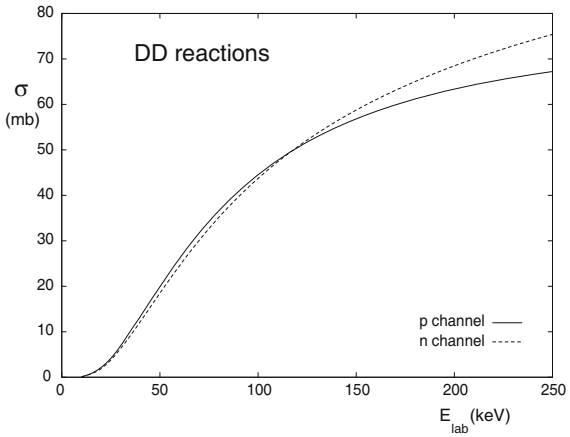

Fig. 19. Integrated cross-sections σ_{tot} of the $^2\mathrm{H}(d,p)^3\mathrm{H}$ and $^2\mathrm{H}(d,n)^3\mathrm{He}$ reactions as functions of the deuteron laboratory energy, as predicted by the Köln T-matrix fit.

are the absolute values and phases of the "internal" (energy independent) matrix elements, normalized such that the integrated cross-sections are in mbarn, the phases are relative to δ_5.

In order to demonstrate the relative strength of the quintet state transitions we compare two S-wave matrix elements γ_1 and δ_1 with the singlet S-wave element α_0 of the $^2\mathrm{H}(d,n)^3\mathrm{He}$ reaction. Table 3 shows them to be of comparable magnitude.

As shown in fig. 18, an explanation for the unexpected strength of quintet transitions can be given by taking transitions via the deuteron D state into account, whereas without the D state quintet transitions could only occur via a Pauli-forbidden spin flip, see *e.g.* [63].

8 Predictions of observables from T-matrix elements

With the results of the T-matrix fit of all available data all observables of the two DD reactions can be predicted. However, one has to keep in mind that despite attempts to avoid ambiguities these cannot be excluded with certainty, even after performing many fit runs with randomly varying starting values. Reconstruction of measured observables is a good test and other predictions must await experimental verification. On the other hand, new data, especially those being underrepresented in the data set (*e.g.*, those consisting of imaginary parts of matrix-element combinations), will help improve the fits. In the following a few examples from the Köln T-matrix analysis will be given.

8.1 Cross-section and analyzing-power observables

Figures 19 and 20 allow to judge the general behaviour of the integrated and differential cross-sections of the two

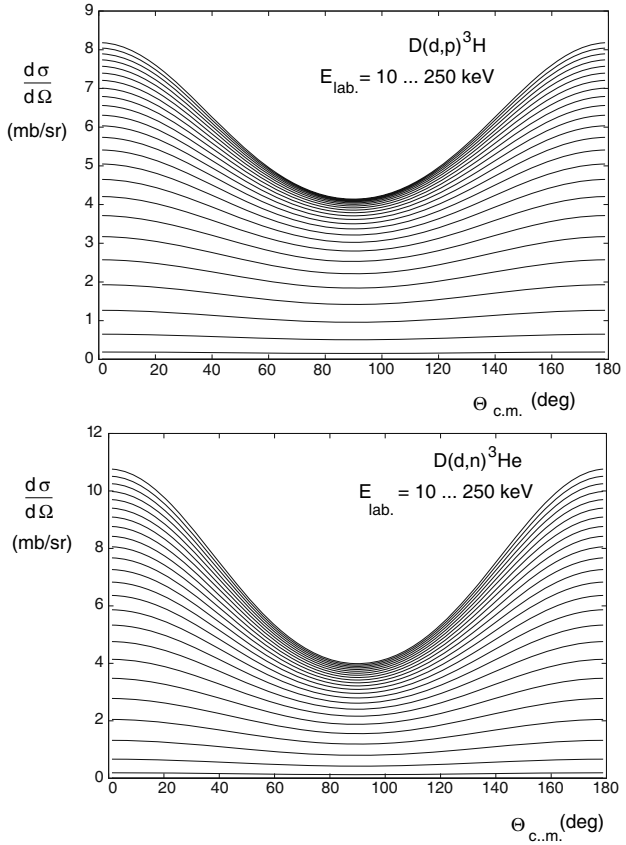

Fig. 20. Differential cross-sections $\mathrm{d}\sigma/\mathrm{d}\Omega$ of the $^2\mathrm{H}(d,p)^3\mathrm{H}$ and $^2\mathrm{H}(d,n)^3\mathrm{He}$ reactions as functions of the deuteron laboratory energy, as predicted by the Köln T-matrix fit.

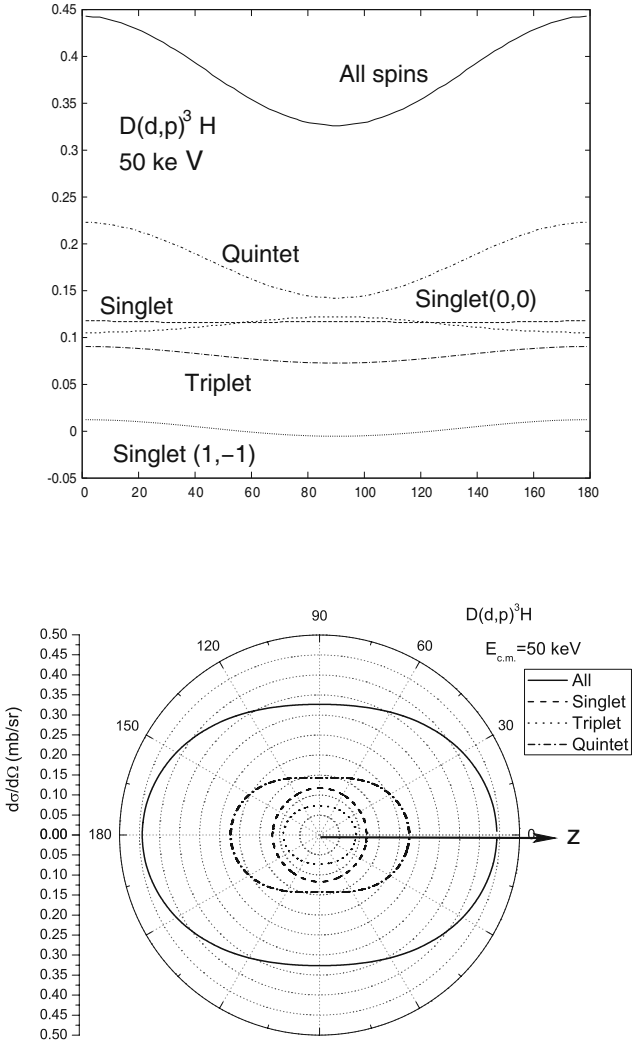

Fig. 21. Angular distribution and polar diagram of the spin-dependent cross-sections of $^2\mathrm{H}(d,p)^3\mathrm{H}$ at $E_{c.m.} = 50\,\mathrm{keV}$ as predicted by the Köln T-matrix fit.

mirror DD reactions with energy and angle, but also the differences between them, which can be attributed to exit-channel Coulomb effects and/or charge-symmetry breaking. It is interesting to distinguish the different contributions to the differential cross-sections from the three (four) possible channel-spin configurations $S = 0$ (two singlet contributions), $S = 1$ (triplet), and $S = 2$ (quintet). This is one of the many possible predictions and delivers information about the directional anisotropies of the reaction products (protons or neutrons). Figure 21 shows this for the $^2\mathrm{H}(d,p)^3\mathrm{H}$ reaction at $E_{lab} = 50\,\mathrm{keV}$. The quintet contribution has the highest anisotropy. For the situation in a fusion-reactor plasma these cross-sections have to be averaged over all directions and the Maxwellian velocity distribution (as in [48]) to obtain the directional dependence of the reaction rates. The following fig. 22 shows predictions for the vector analyzing power A_y for both reactions as functions of energy and angle. In the following only a few examples of the fit results together with data will be shown. σ_{tot} and Legendre anisotropy coefficients of $\mathrm{d}\sigma/\mathrm{d}\Omega$ and A_y as functions of the laboratory deuteron energy for the $^2\mathrm{H}(d,p)^3\mathrm{H}$ reaction, same for tensor analyzing powers, are compared with experimental data in figs. 23 and 24. The comparisons with the smoothly varying fit results expose the partly good, but in some cases also quite bad, quality of the available data (see also ref. [44]).

8.2 Quintet suppression factor (QSF)

Figure 25 summarizes all results for the QSF from different theoretical predictions as well as two data parametrizations for both DD reactions. The energy range covers the fusion energy range up to 500 keV. It can be seen that the behavior derived from experimental results shows no or very little neutron suppression in the quintet state in the relevant energy region, but also the appreciable differences between the two approaches. It is interesting that substantial suppression occurs for the other two spin configurations, especially at very low energies (below $\approx$ 150 keV laboratory energy) for the triplet state and at the higher energies (above $\approx$ 100 keV laboratory energy) for the singlet state, as shown in fig. 26. The results depicted in figs. 25 and 26 show that the (indirectly obtained, *i.e.* predicted) data are at variance with all theoretical predictions and favor *no* quintet state suppression. A plausible

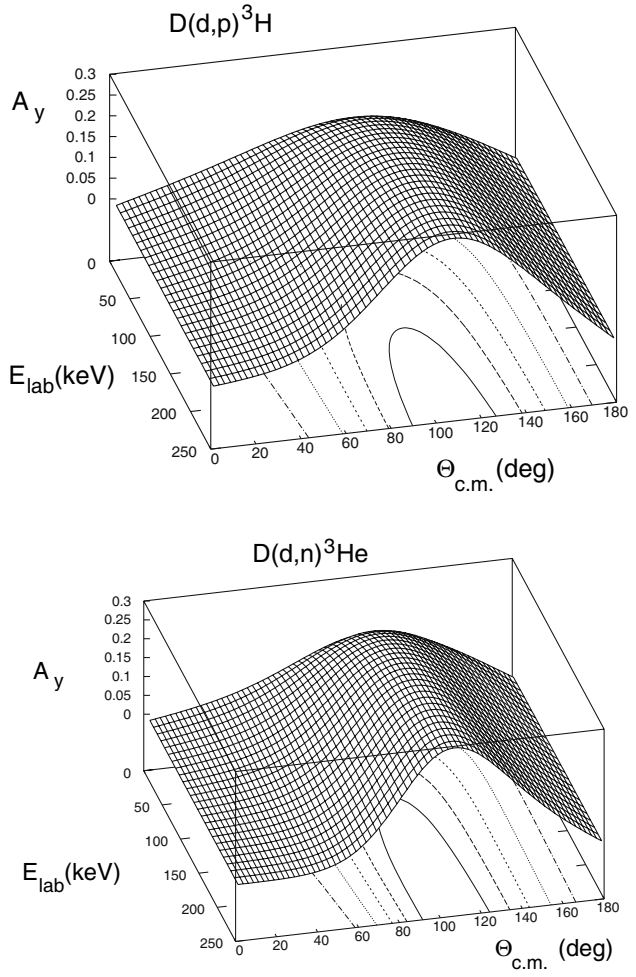

Fig. 22. Vector analyzing powers of $^2\mathrm{H}(d,p)^3\mathrm{H}$ and $^2\mathrm{H}(d,n)^3\mathrm{He}$ as predicted by the Köln T-matrix fit.

explanation of this behaviour has been given above and illustrated by fig. 18.

8.3 Spin correlation

No low-energy data of spin correlations of the two DD reactions exist. Such data are, however, needed not only to improve the matrix-element fits but especially for our knowledge on possible neutron suppression.

The (differential) cross-section (in spherical notation) of a reaction of a spin-1 particle beam (a) with a spin-1 target (A) (such as for the DD reactions) reads

$$\sigma_{pol}(\Theta,\Phi) = \sigma_0(\Theta) \sum_{k_A q_A, k_a q_a} t_{k_A q_A} t_{k_a q_a} C^*_{k_A q_A, k_a q_a},$$

C is a special case of the "generalized analyzing power":

$$C_{k_A q_A, k_a q_a} = (\Xi^{00,00}_{k_A q_A, k_a q_a})^*$$

when no outgoing polarizations, but only intensities are measured. The ingoing polarization tensor, with polarizations of beam and target being prepared independently,

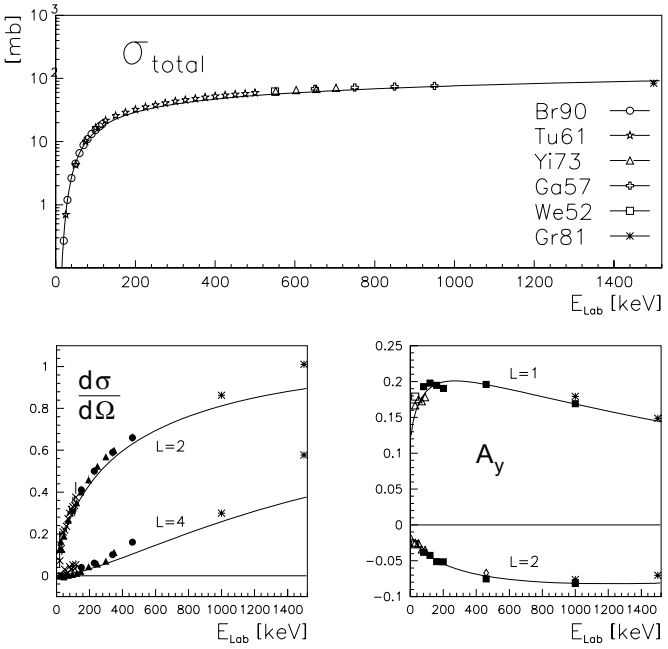

Fig. 23. Köln fit to σ_{tot} (top) and Legendre anisotropy coefficients of $\mathrm{d}\sigma/\mathrm{d}\Omega$ (lower left) and A_y (lower right) of the $^2\mathrm{H}(d,p)^3\mathrm{H}$ reaction as functions of the deuteron laboratory energy. The data points from different sources are explained in [51,52]. The L-values designate the order of the relevant Legendre polynomial or Legendre function of the Legendre expansions.

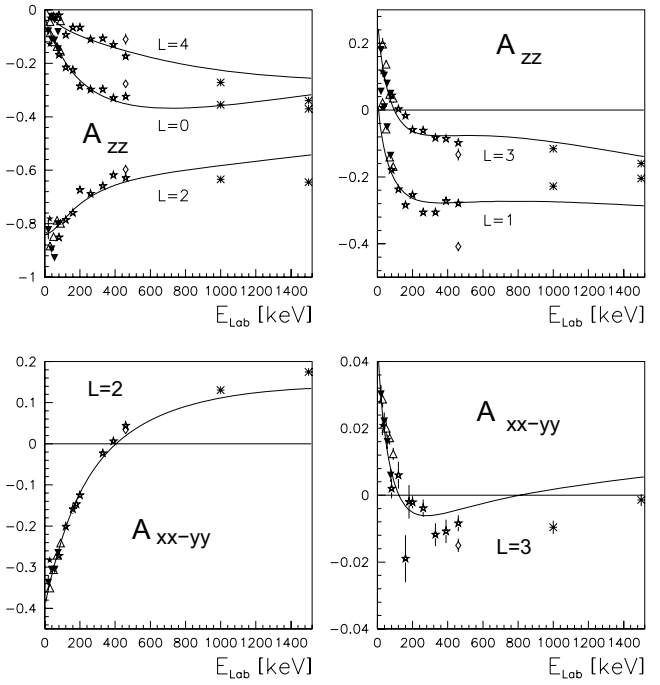

Fig. 24. Köln fit to different Legendre expansion coefficients of tensor analyzing powers of the $^2\mathrm{H}(d,p)^3\mathrm{H}$ reaction as functions of the deuteron laboratory energy. The L-values are again the orders of the relevant Legendre polynomials or functions.

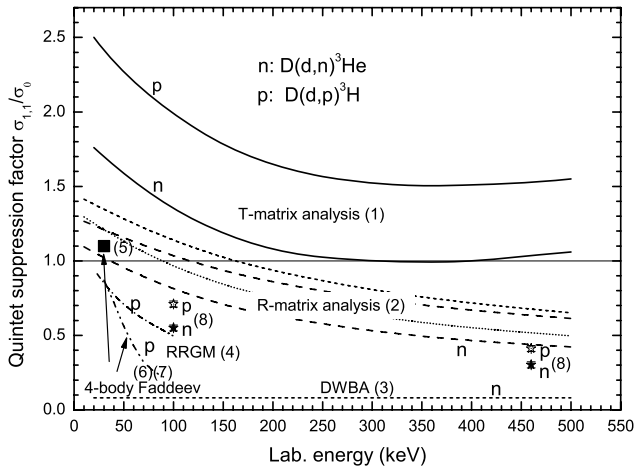

Fig. 25. Quintet suppression factor as predicted by various theoretical and from two experimental approaches using world data of DD reactions. The relevant references (numbers in parentheses in the figure) are: (1) [50]; (2) [48,43]; (3) [64, 65]; (4) [66,67]; (5) [35]; (6) [68]; (7) [69] and (8) [37,70]. The predictions from refs. [35,68,70] are from microscopic Faddeev-Yakubovsky calculations.

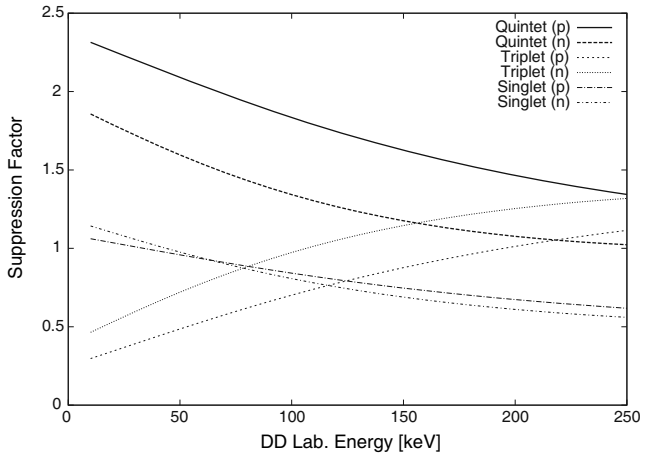

Fig. 26. Suppression factors for different spin states of $^2\mathrm{H}(d,p)^3\mathrm{H}$ and $^2\mathrm{H}(d,n)^3\mathrm{He}$ as predicted by using matrix elements from the T-matrix fit of [50–52].

factorizes into a product of both tensors. With all terms allowed by parity conservation and hermiticity we get [51]

$$
\begin{aligned}
&[\sigma_{pol}(\Theta,\Phi)]_{\Phi=0} = \sigma_0(\Theta)\{1 + 2[iC_{00,11}(\Theta)\Re(it_{00,11})\\
&+iC_{11,00}(\Theta)\Re(it_{11,00})]\\
&+[C_{00,20}(\Theta)t_{00,20} + C_{20,00}(\Theta)t_{20,00}]\\
&+2[C_{00,21}(\Theta)t_{00,21} + C_{21,00}(\Theta)t_{21,00}]\\
&+2[C_{00,22}(\Theta)t_{00,22} + C_{22,00}(\Theta)t_{22,00}] + C_{10,10}(\Theta)t_{10,10}\\
&+2[C_{10,11}(\Theta)t_{10,11} + C_{11,10}(\Theta)t_{11,10}]\\
&+2[iC_{10,21}(\Theta)\Re(it_{10,21}) + iC_{21,10}(\Theta)\Re(it_{21,10})]\\
&+2[iC_{10,22}(\Theta)\Re(it_{10,22})\\
&+iC_{22,10}(\Theta)\Re(it_{22,10})] + 4C_{11,11}t_{11,11}\\
&+2[iC_{11,20}(\Theta)\Re(it_{11,20}) + iC_{20,11}(\Theta)\Re(it_{20,11})]\\
&+4[iC_{11,21}(\Theta)\Re(it_{11,21}) + iC_{21,11}(\Theta)\Re(it_{21,11})]\\
&+4[iC_{11,22}(\Theta)\Re(it_{11,22})\\
&+iC_{22,11}(\Theta)\Re(it_{22,11})] + C_{20,20}t_{20,20}\\
&+2[C_{20,21}(\Theta)t_{20,21} + C_{21,20}(\Theta)t_{21,20}\\
&+C_{20,22}(\Theta)t_{20,22} + C_{22,20}(\Theta)t_{22,20}]\\
&+4[C_{21,21}(\Theta)t_{21,21} + C_{21,22}(\Theta)t_{21,22}\\
&+C_{22,21}(\Theta)t_{22,21}] + 4C_{22,22}(\Theta)t_{22,22}\}.
\end{aligned}
$$

This cross-section expressed in Cartesian coordinates is

$$
\begin{aligned}
&[\sigma(\Theta,\Phi)]_{\Phi=0} = \sigma_0(\Theta)\Big\{1 + \frac{3}{2}\left[A_y^{(b)}(\Theta)p_y + A_y^{(t)}q_y\right]\\
&+\frac{1}{2}\left[A_{zz}^{(b)}(\Theta)p_{zz} + A_{zz}^{(t)}(\Theta)q_{zz}\right]\\
&+\frac{1}{6}\left[A_{xx-yy}^{(b)}(\Theta)p_{xx-yy} + A_{xx-yy}^{(t)}(\Theta)q_{xx-yy}\right]\\
&+\frac{2}{3}\left[A_{xz}^{(b)}(\Theta)p_{xz} + A_{xz}^{(t)}(\Theta)q_{xz}\right] + \frac{9}{4}\left[C_{y,y}(\Theta)p_yq_y\right.\\
&+C_{x,x}(\Theta)p_xq_x + C_{x,z}(\Theta)p_xq_z\\
&+C_{z,x}(\Theta)p_zq_x + C_{z,z}(\Theta)p_zq_z]\\
&+\frac{3}{4}\left[C_{y,zz}(\Theta)p_yq_{zz} + C_{zz,y}(\Theta)p_{zz}q_y\right]\\
&+C_{y,xz}(\Theta)p_yq_{xz} + C_{xz,y}(\Theta)p_{xz}q_y + C_{x,yz}(\Theta)p_xq_{yz}\\
&+C_{yz,x}(\Theta)p_{yz}q_x + C_{z,yz}(\Theta)p_zq_{yz} + C_{yz,z}(\Theta)p_{yz}q_z\\
&+\frac{1}{4}\left[C_{y,xx-yy}(\Theta)p_yq_{xx-yy} + C_{xx-yy,y}(\Theta)p_{xx-yy}q_y\right.\\
&+C_{zz,zz}(\Theta)p_{zz}q_{zz}] + \frac{1}{3}\left[C_{zz,xz}(\Theta)p_{zz}q_{xz}\right.\\
&+C_{xz,zz}(\Theta)p_{xz}q_{zz}] + \frac{1}{12}\left[C_{zz,xx-yy}(\Theta)p_{zz}q_{xx-yy}\right.\\
&+C_{xx-yy,zz}(\Theta)p_{xx-yy}q_{zz}]\\
&+\frac{4}{9}\left[C_{xz,xz}(\Theta)p_{xz}q_{xz} + C_{yz,yz}(\Theta)p_{yz}q_{yz}\right]\\
&+\frac{8}{9}\left[C_{xy,yz}(\Theta)p_{xy}q_{yz} + C_{yz,xy}(\Theta)p_{yz}q_{xy}\right]\\
&+\frac{16}{9}C_{xy,xy}(\Theta)p_{xy}q_{xy} + \frac{1}{9}\left[C_{xz,xx-yy}(\Theta)p_{xz}q_{xx-yy}\right.\\
&+C_{xx-yy,xz}(\Theta)p_{xx-yy}q_{xz}]\\
&+\frac{1}{36}C_{xx-yy,xx-yy}(\Theta)p_{xx-yy}q_{xx-yy} + \frac{1}{2}\left[C_{x,xy}(\Theta)p_xq_{xy}\right.\\
&\left.\left.+C_{xy,x}(\Theta)p_{xy}q_x + C_{z,xy}(\Theta)p_zq_{xy} + C_{xy,z}(\Theta)p_{xy}q_z\right]\right\}.
\end{aligned}
$$

The $C_{k_Aq_A,k_aq_a}$ or the $C_{i,i'}$ $(i,i' = x,y,z,xx,xy,\ldots)$, respectively, are the spin-correlation coefficients, the $C_{k_Aq_A,00}$, C_{00,k_aq_a} and A_i analyzing powers, the $t_{k_aq_a}$ or $p_{ii'}$ beam and the $t_{k_Aq_A}$ or $q_{ii'}$ target polarization components. Again due to overcompleteness of this equation several relations between the correlation coefficients result:

$$C_{xx,i} + C_{yy,i} + C_{zz,i} = 0 \quad \text{and} \quad C_{i,xx} + C_{i,yy} + C_{i,zz} = 0.$$

The observables (analyzing powers or spin-correlation coefficients) depend on the polar angle Θ. This dependence is introduced by the nuclear dynamics, see the above

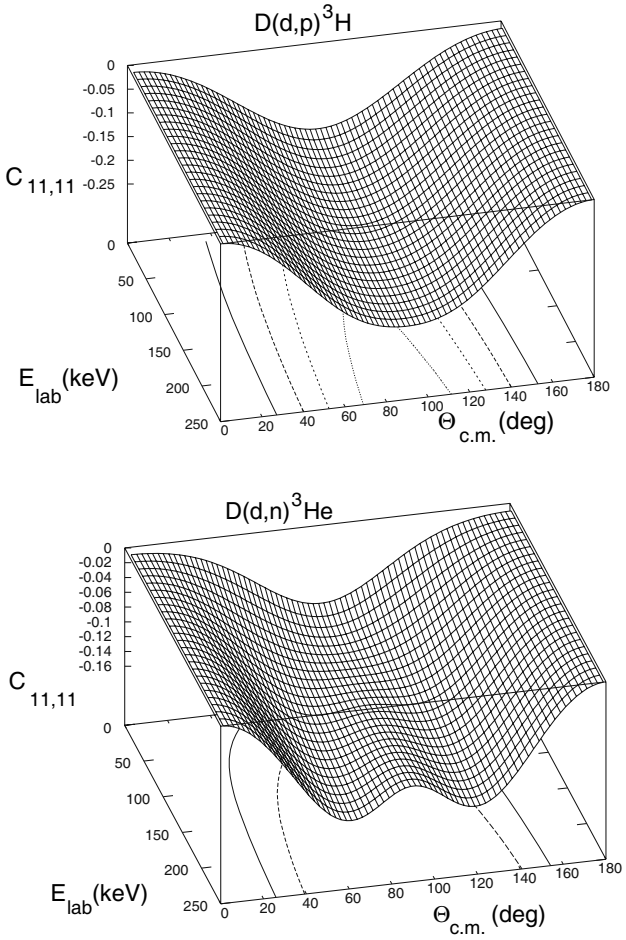

Fig. 27. Spin-correlation coefficient $C_{11,11}$ of the reactions $^2\vec{\mathrm{H}}(\vec{d},p)^3\mathrm{H}$ and $^2\vec{\mathrm{H}}(\vec{d},n)^3\mathrm{He}$ for low energies, as predicted by the Köln T-matrix analysis.

formula by Welton [53]. The necessary introduction of coordinate systems, *e.g.* the often used helicity frames [11] together with following the *Madison Convention* [56] leads to a Φ-dependence of the cross-section (not of the observables!). The y-axis is usually defined along the vector $\vec{k}_{in} \times \vec{k}_{out}$, *i.e.* depends on the direction of each detector, with the z-axis, *e.g.*, along $\vec{k}_{in}$ and forming a right-handed coordinate system with x. The projection of the spin (symmetry) axis onto the x-y plane forms the angle Φ with the y-axis. It is obvious that for entrance channel-spin correlations in principle two such systems can be defined leading to two different Φ-dependences [11]. In the above formulae Φ has been set to 0, corresponding to both (target and beam) polarization vectors along the same y-axis.

Since analyzing powers for beam or target polarizations are also part of the correlation cross-section they must be separately measured or entered from known data. For the measurements simplifications will be possible by utilizing the possibilities of the beam and target sources of producing pure vector or tensor polarizations and of orienting the polarization direction (direction of the polarization vector) by electrostatic beam deflection or with the

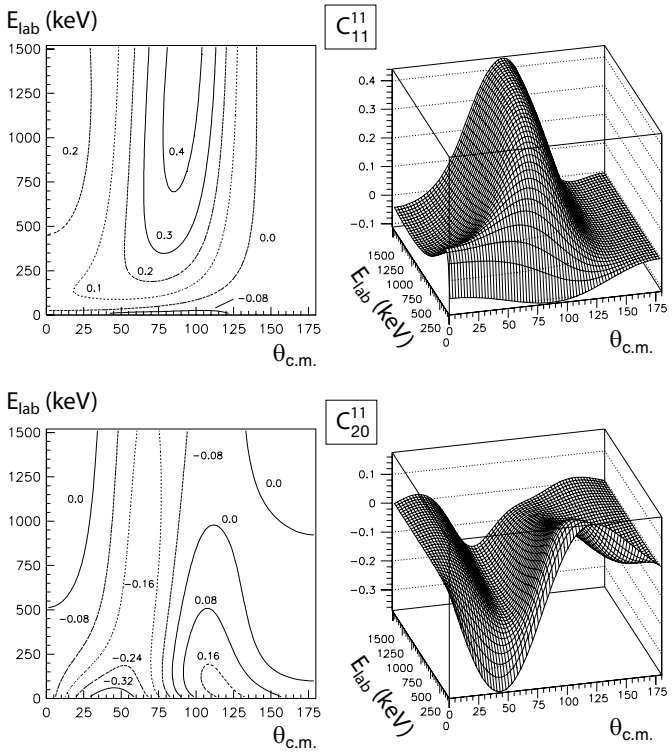

Fig. 28. Polarization transfer coefficients C_{11}^{11} and C_{20}^{11} of the reaction $^2\mathrm{H}(\vec{d},\vec{p})^3\mathrm{H}$, predicted by the Köln T-matrix analysis.

help of magnetic fields (Wien filters and spin precession in dipole magnets) along the x, y, and z axes. Assuming that the polarization symmetry axes both coincide, *e.g.*, in the z-axis direction one obtains

$$\sigma(\Theta,\Phi) = \sigma_0(\Theta)\left\{1 + \frac{3}{2}\left[A_{zz}^{(b)}(\Theta)p_{zz} + A_{zz}^{(t)}(\Theta)q_{zz}\right] + \frac{9}{4}C_{z,z}(\Theta)p_z q_z + \frac{1}{4}C_{zz,zz}(\Theta)p_{zz}q_{zz}\right\}.$$

The Köln T-matrix analysis can be used to make predictions of these correlation coefficients. As an example in fig. 27 we plot the vector-vector polarization correlation coefficient $C_{11,11}$ as a function of energy from 10 to 250 keV (lab.) and c.m. angle. The figure shows the relatively weak energy dependence of the correlation coefficient and the onset of the influence of D-wave contributions at the higher energies, slightly different for both reactions. A complete set of c.m. angular distributions of all observables relevant for spin-correlation measurements for all laboratory energies between 10 and 250 keV in 10 keV steps is shown in appendix A (figs. 35–45).

8.4 Polarization transfer

Here very few data exist. Figure 28 gives a prediction for two of many polarization transfer coefficients in the low-energy range as functions of angle and energy. It is clearly desirable to amend the existing data set by new data. Two

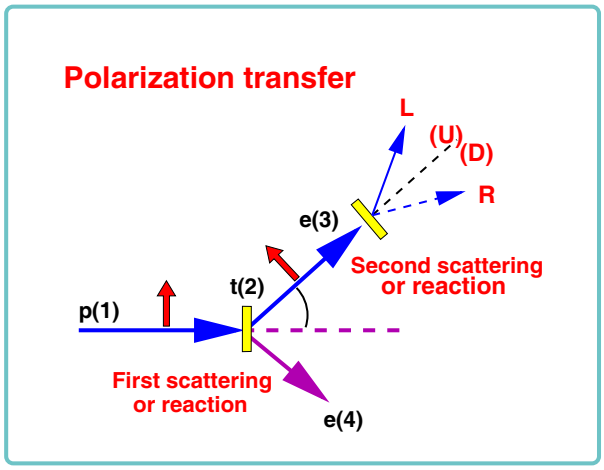

Fig. 29. Scheme of a polarization transfer measurement. For the ^{2}H$(d,p)^3$H reaction the incident deuteron (particle 1) can be vector and/or tensor polarized and the vector polarization of the outgoing proton (ejectile 3) will be measured. Note that in principle, *i.e.* without restrictions due to symmetries such as parity conservation, the polarization in the entrance channel can be prepared or, in the outgoing channel, can be measured in three spatial directions leading to a corresponding number of polarization transfer coefficients. Symmetries reduce the number of independent coefficients.

new measurements of the polarization transfer coefficient $K_y^{y'}$ have recently been published. They were motivated by the calculated predictions, together with the need to obtain a more balanced set of input data to the matrix-element analysis [71,72]. However, these data have not yet been included in a new T-matrix fit and can therefore only be compared to the existing prediction.

The principle of polarization transfer experiments will be explained briefly. Figure 29 shows the scheme of a polarization transfer measurement whereas the following equations give the relations between the polarization components of the ejectiles of the first reaction, to be measured by a second scattering, and the incident polarization. The K's are the relevant tranfer coefficients in Cartesian notation. For a vector-to-vector polarization transfer, *e.g.* for D$(\vec{d},\vec{p})^3$H we have

$$p_{x'} = \frac{p_x K_x^{x'} + p_z K_z^{x'}}{1 + p_y A_y},$$

$$p_{y'} = \frac{A_y + p_y K_y^{y'}}{1 + p_y A_y},$$

$$p_{z'} = \frac{p_x K_x^{z'} + p_z K_z^{z'}}{1 + p_y A_y}.$$

By taking countrate ratios between differently prepared projectile polarizations (*e.g.*, up/down) and for different polarimeter detectors (up/down/left/right) the polarization transfer coefficients, *e.g.* $K_y^{y'}$ and $K_z^{x'}$ are obtained. For illustration we show in fig. 30 a typical experimental setup of a polarization transfer polarimeter as used recently [72].

In fig. 31 the two new data points are compared to the only existing microscopic calculation and to predictions of the T-matrix analysis.

8.5 Other recent experimental data

Besides the new polarization transfer data of ^{2}H$(d,p)^3$H discussed above only one set of new data has been published recently. These new data consist of precise differential cross-sections of the ^{2}H$(d,p)^3$H and the ^{2}H$(d,n)^3$He reactions measured recently at TUNL in an energy range where very few data exist [73], *i.e.* for eight deuteron laboratory energies between 112.2 and 646.1 keV. These data are urgently needed, not only for nuclear astrophysics (*i.e.* big-bang nucleosynthesis). In fig. 32 we show an example at 655 keV.

9 Outlook and proposal for "polarized fusion"

It is not clear when realistic microscopic calculations (Faddeev-Yakubovsky and/or χPT + Coulomb) will become available for the fusion energy range. In view of this situation, but also independently, a direct measurement of the quintet suppression factor seems mandatory. Although announced, such polarization correlation cross-sections have not been measured yet, and their measurement meets formidable difficulties. The main problem is caused by the low cross-sections. The use of a polarized solid deuterium target is also very difficult and has the danger of contaminations from reaction products from other target constituents.

The cleanest solution seems to be the use of two polarized beams of maximum intensity colliding in the detection region. Completely new designs and development work could be avoided by using and modifying existing equipment such as from the sources developed at HERMES/DESY, ANKE/COSY Jülich or at the Köln tandem accelerator. Such a procedure was suggested recently [74,75]. One beam could be the polarized atomic beam from an atomic-beam source such as developed for SAPIS, [76], as shown in fig. 33, or from the KVI (Groningen) source. The second beam could be obtained by ionizing the atomic beam after crossing the interaction region in an electron collision ionizer of the Glavish type and recirculating the ions to cross the interaction region perpendicularly to the original atomic beam. This will require a careful design of the beam optics to avoid any beam losses. On the other hand, the colliding target beam could be another atomic beam from a similar atomic-beam source or even from a charged-particle source such as the old Köln Lambshift source LASCO [77], see fig. 34. The Lambshift source could be run either with negative polarized ions using the established scheme of charge exchange of the metastables on argon or the never-used but also

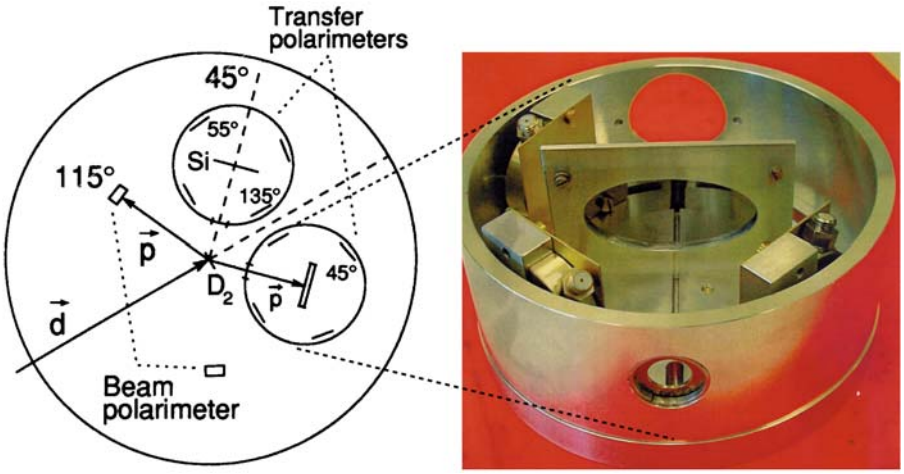

Fig. 30. Low-energy experimental setup of the Köln polarization transfer measurement. Two Si polarimeters, left and right, were mounted inside an ORTEC 600 scattering chamber together with beam polarization monitors. Primary targets consisted of TiD_x foils, whereas Si foils served as second (polarimeter) scatterers. For details see ref. [72].

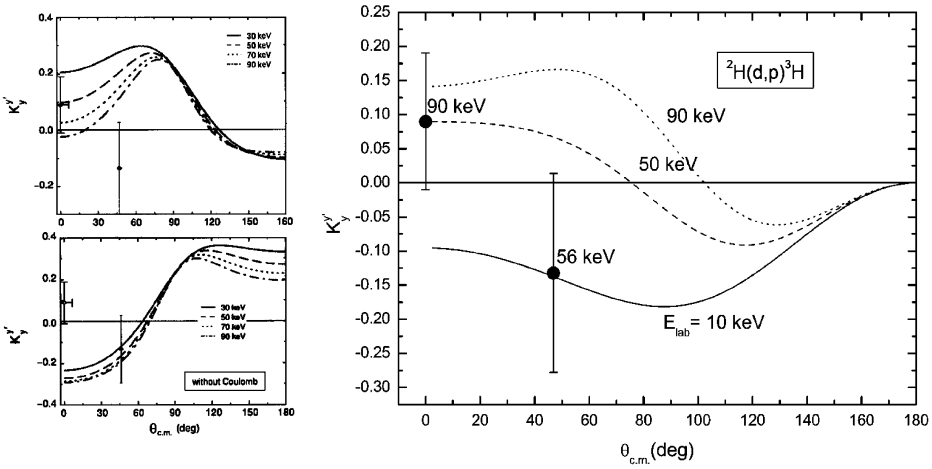

Fig. 31. Left: our result ($\theta_{c.m.} = 47°$), compared to Katabuchi's result ($\theta_{c.m.} = 0°$) and calculations by Uzu —with and without Coulomb modification [68]. Right: experimental results compared to T-matrix fit predictions using Geiger's matrix elements.

well-established scheme of ionization of the metastables on iodine vapor leading to positive ions with a figure of merit twice that for the negative ions [78,79]. The two-sources scheme offers better flexibility for spin handling and probably higher collision rates. However, in any case the count rates will be very low (≈ 1 per 100 s) which requires long-term stable and more or less automated measurements. The background from cosmic rays, terrestrial radioactivity, and from electronic disturbances will be a matter of concern.

The quantities to be measured (among others) would have to be angular distributions of the differential spin-correlation cross-sections with different combinations of the three possible polarization directions of both beams. Simplifications of the experiment are possible not only by choosing x, y, and z polarization directions but also by the possibility of choosing pure vector or tensor polarization for the beams.

From the differential cross-sections —by integration over the full angular range— the integrated polarization

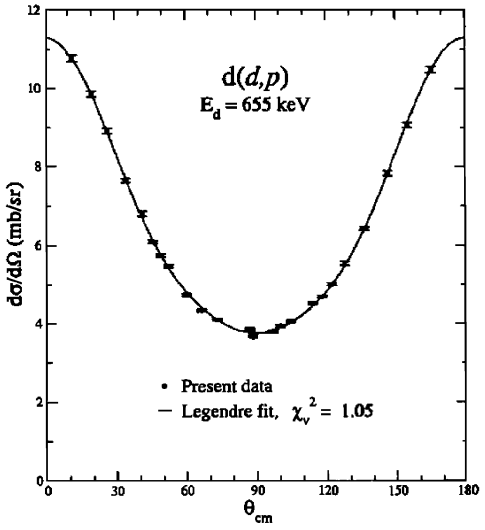

Fig. 32. Differential cross-section of the $^2H(d,p)^3H$ reaction at 655 keV (From [73] by permission of APS.)

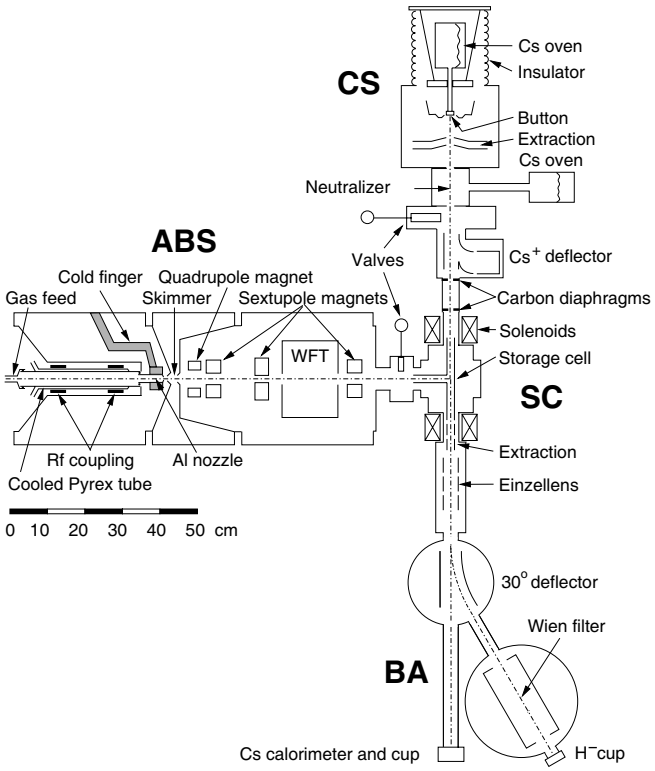

Fig. 33. Stored Atoms Polarized Ion Source (SAPIS). ABS = atomic beam source, CS = cesium beam source, SC = storage cell, BA = beam analysis.

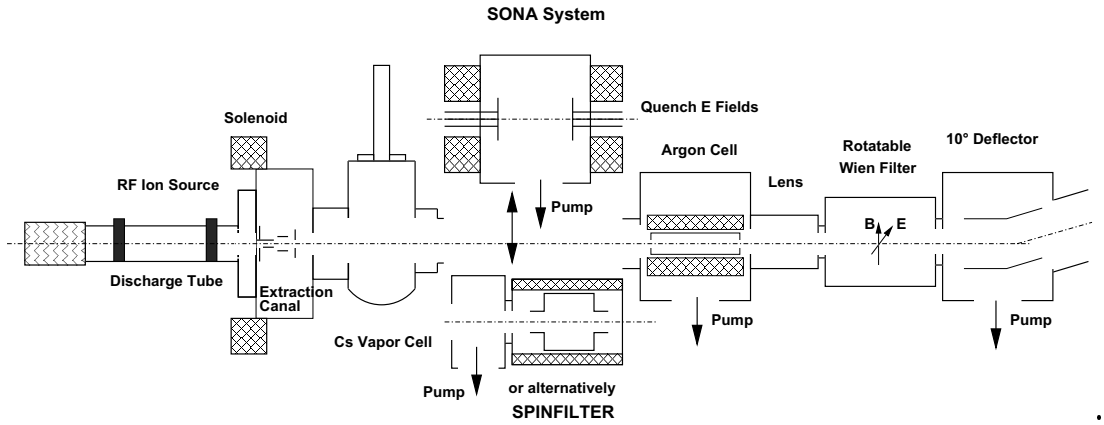

Fig. 34. The Köln Lambshift source LASCO [77]. The source produced negative H or D ions with polarizations up to 75% of the ideal theoretical values and currents up to 400 nA (H), 600 nA (D).

correlation cross-sections are obtained from which the QSF is derived. For the measurements, arrays of solid-state detectors around the collision region covering as much of the available phase space as possible appear suitable. The polarizations of both beams must be measured. For the atomic beam the Köln/Jülich Lambshift polarimeter [80] is an ideal device whereas for the charged-particle beams the classical low-energy nuclear reactions may be used: ^{2}H$(d,p)^3$H, ^{2}H$(d,n)^3$He, ^{3}H$(d,n)^4$He, and ^{3}He$(d,p)^4$He. The classical analyzer reactions used at higher energies, such as ^{4}He$(d,d)^4$He and ^{12}C$(d,d)^{12}$C, have too small polarimeter figures of merit.

I want to thank R. Engels, A. Vassiliev, and S. Sherman for valuable discussions. The support by Deutsche Forschungsgemeinschaft DFG (Project No. DD000074) is gratefully acknowledged.

Appendix A. Predictions of observables

We show in figs. 35–45 a complete set of c.m. angular distributions of all observables relevant for spin-correlation measurements for all laboratory energies between 10 and 250 keV in 10 keV steps.

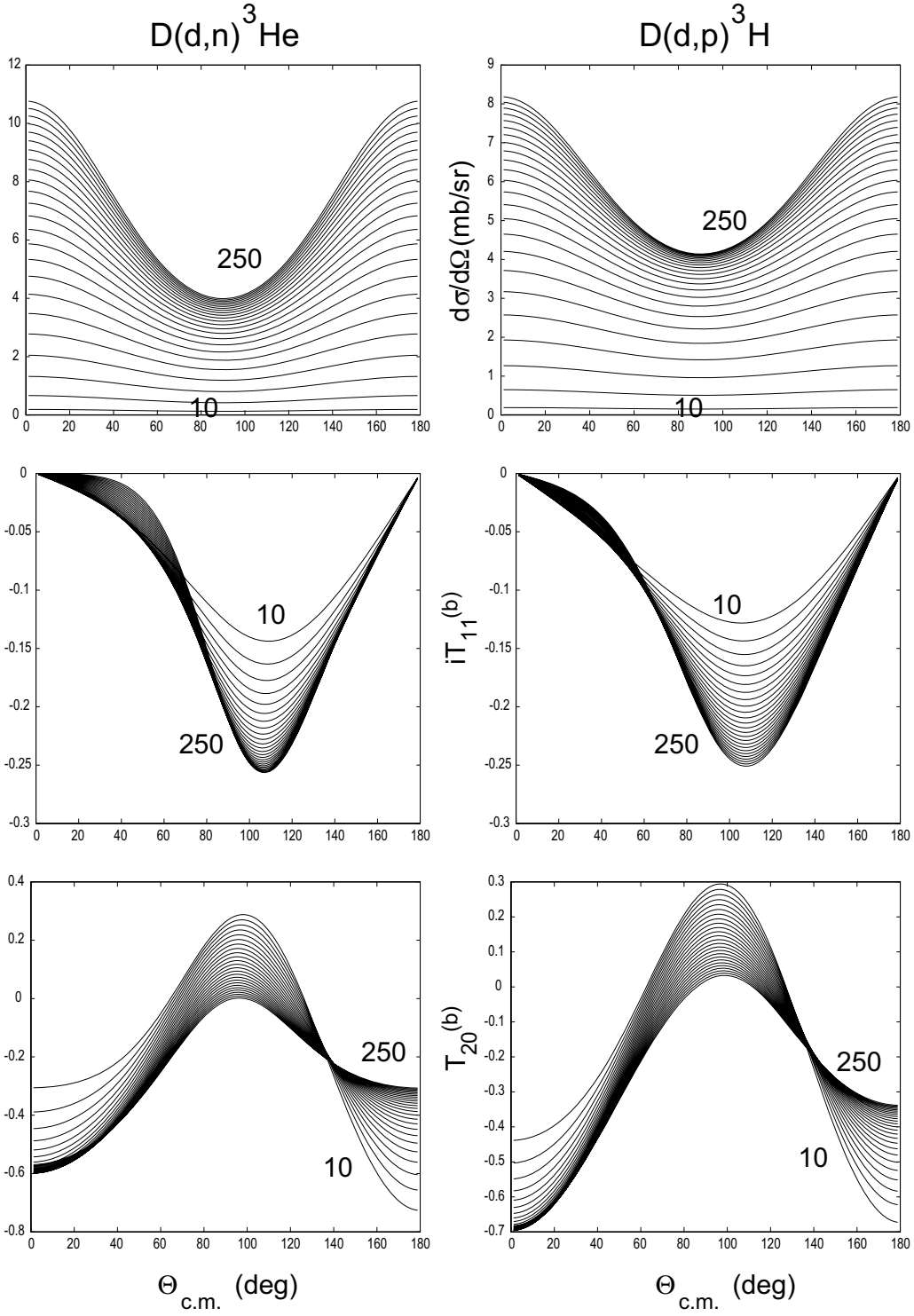

Fig. 35. Predictions with the Köln matrix elements of differential (unpolarized) cross-sections and beam (b) analyzing powers for laboratory energies from 10 to 250 keV in 10 keV steps.

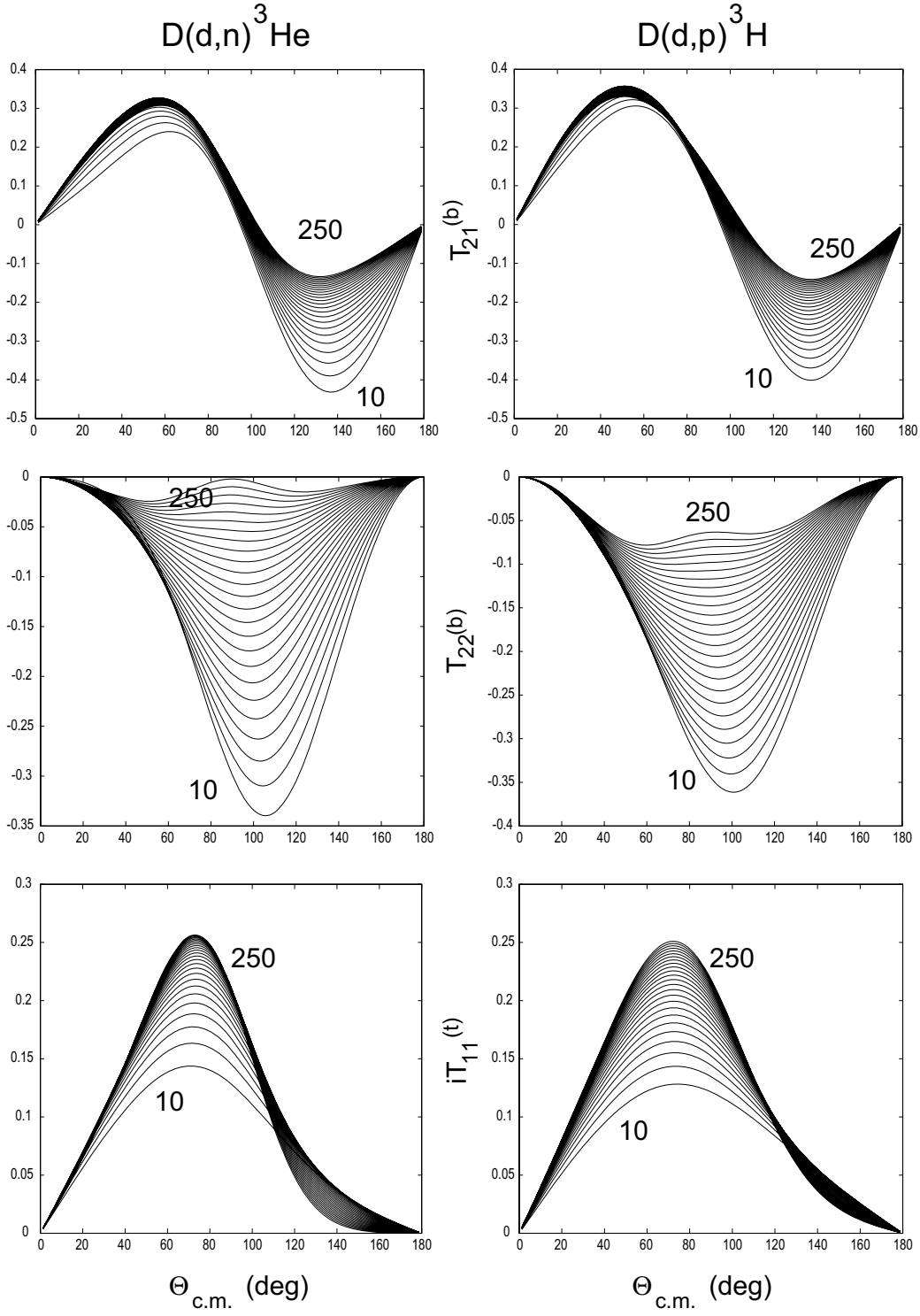

Fig. 36. Predictions with the Köln matrix elements of beam (b) and target (t) analyzing powers for laboratory energies from 10 to 250 keV in 10 keV steps.

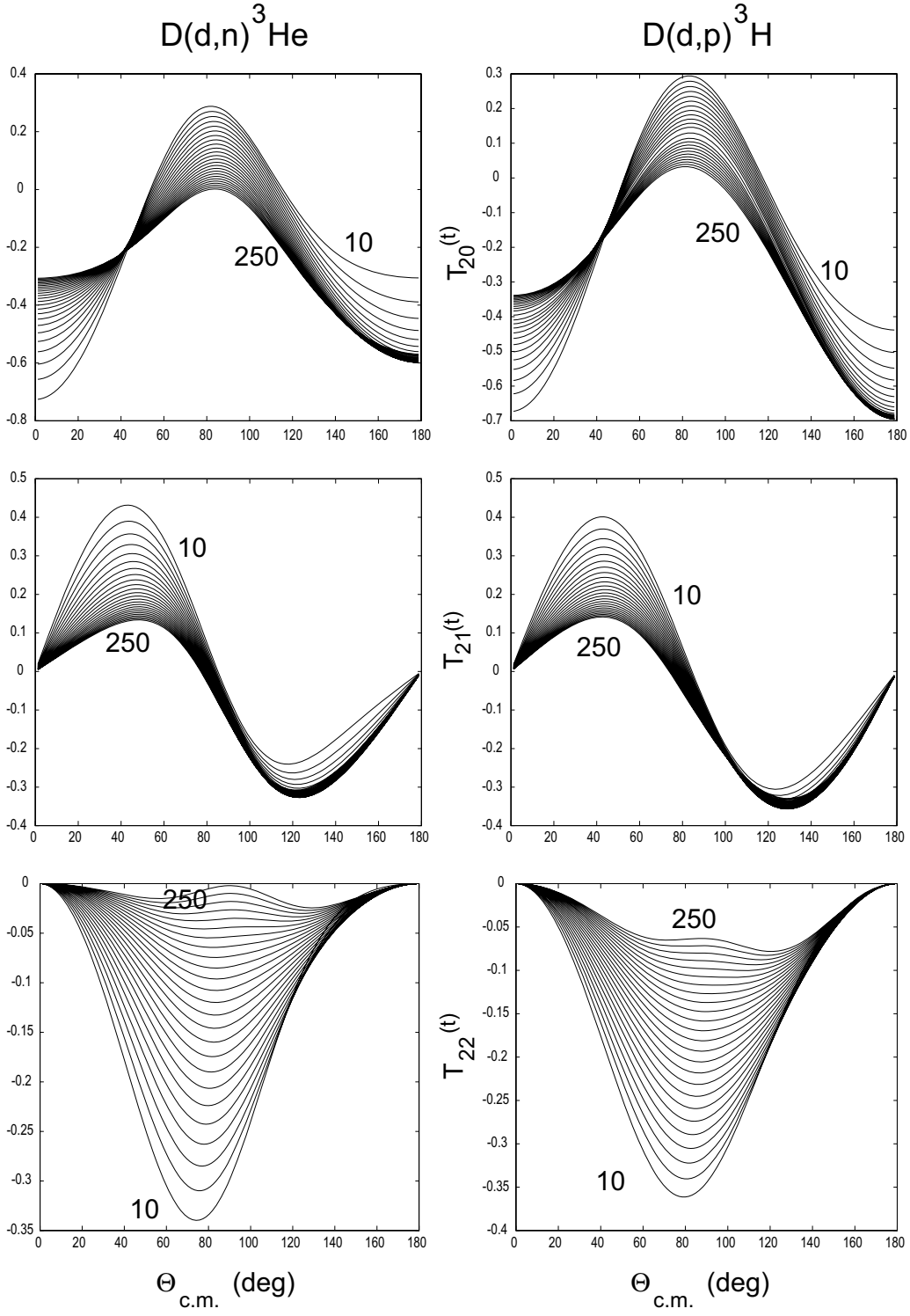

Fig. 37. Predictions with the Köln matrix elements of target (t) analyzing powers for laboratory energies from 10 to 250 keV in 10 keV steps.

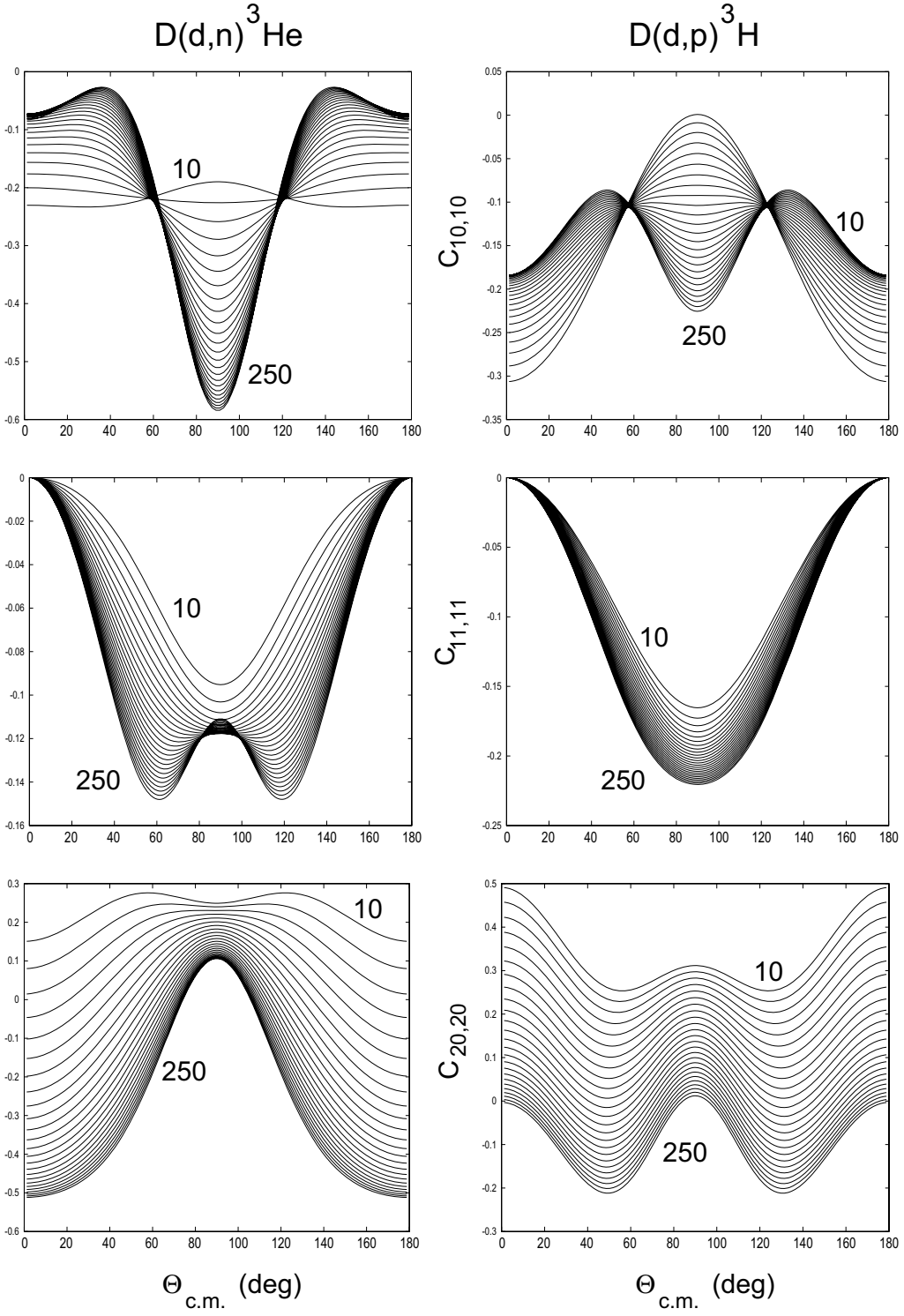

Fig. 38. Predictions with the Köln matrix elements of spin correlations for laboratory energies from 10 to 250 keV in 10 keV steps. The first two indices are for the target polarization state, the last two for the beam.

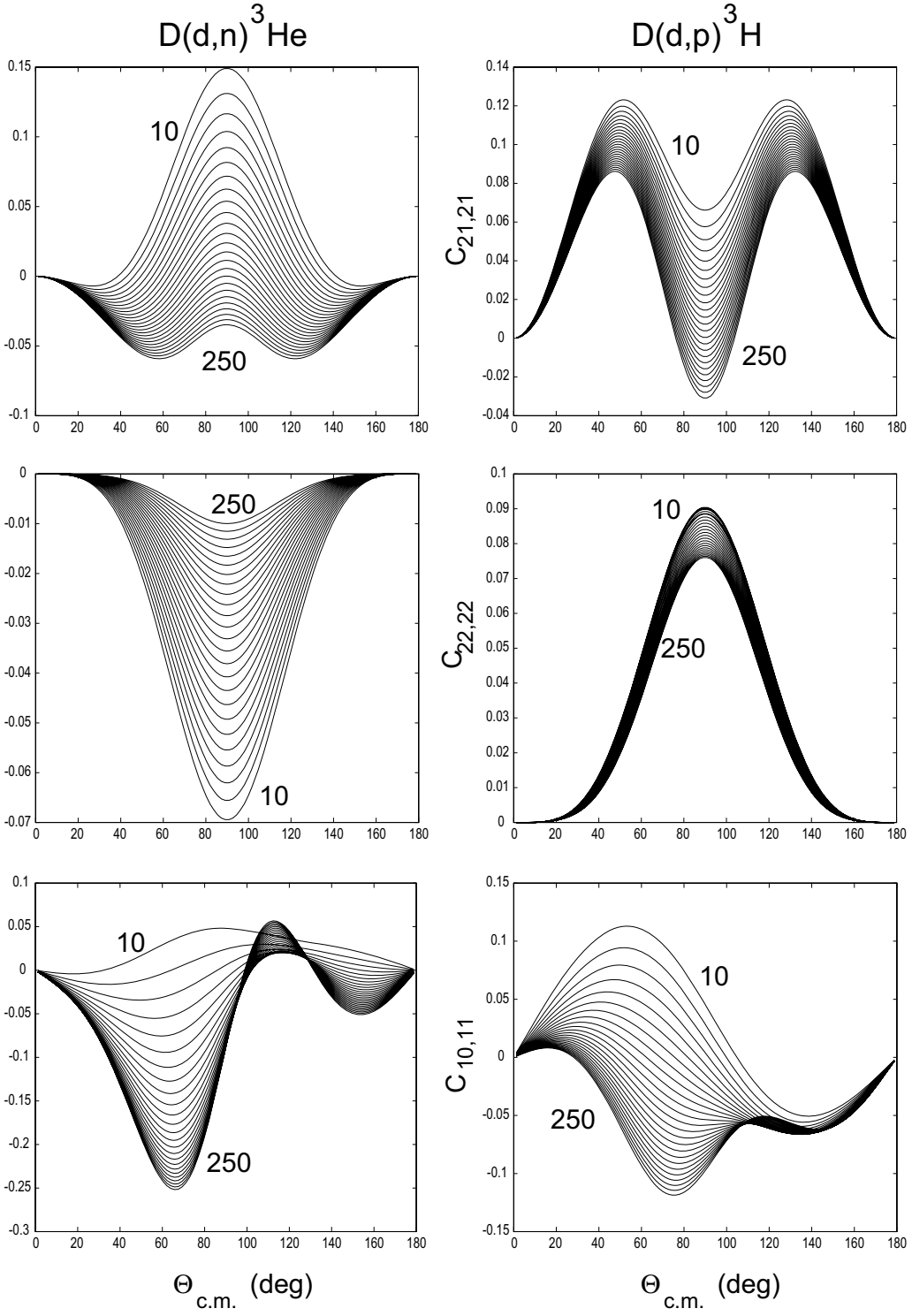

Fig. 39. The same as fig. 38.

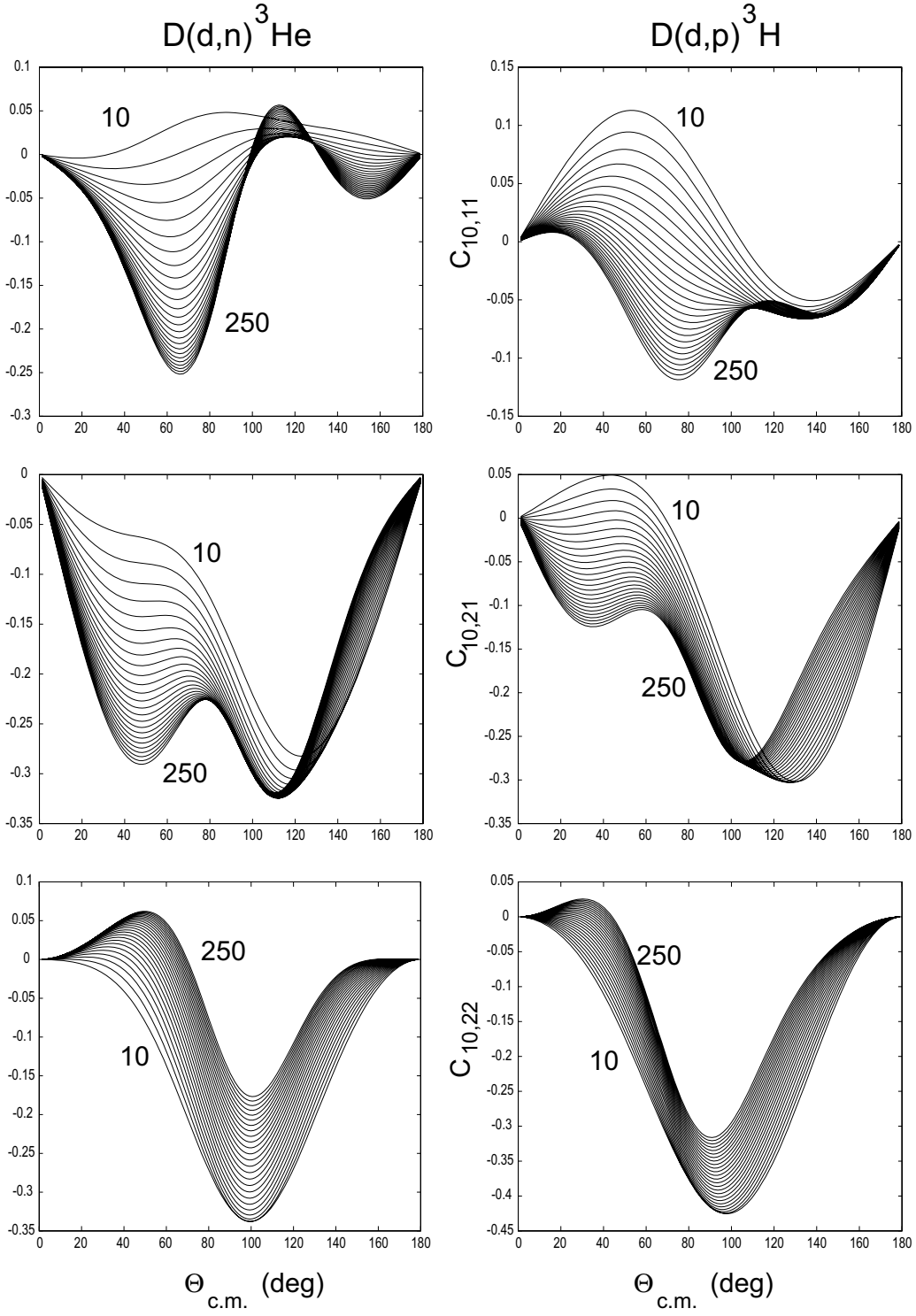

Fig. 40. The same as fig. 38.

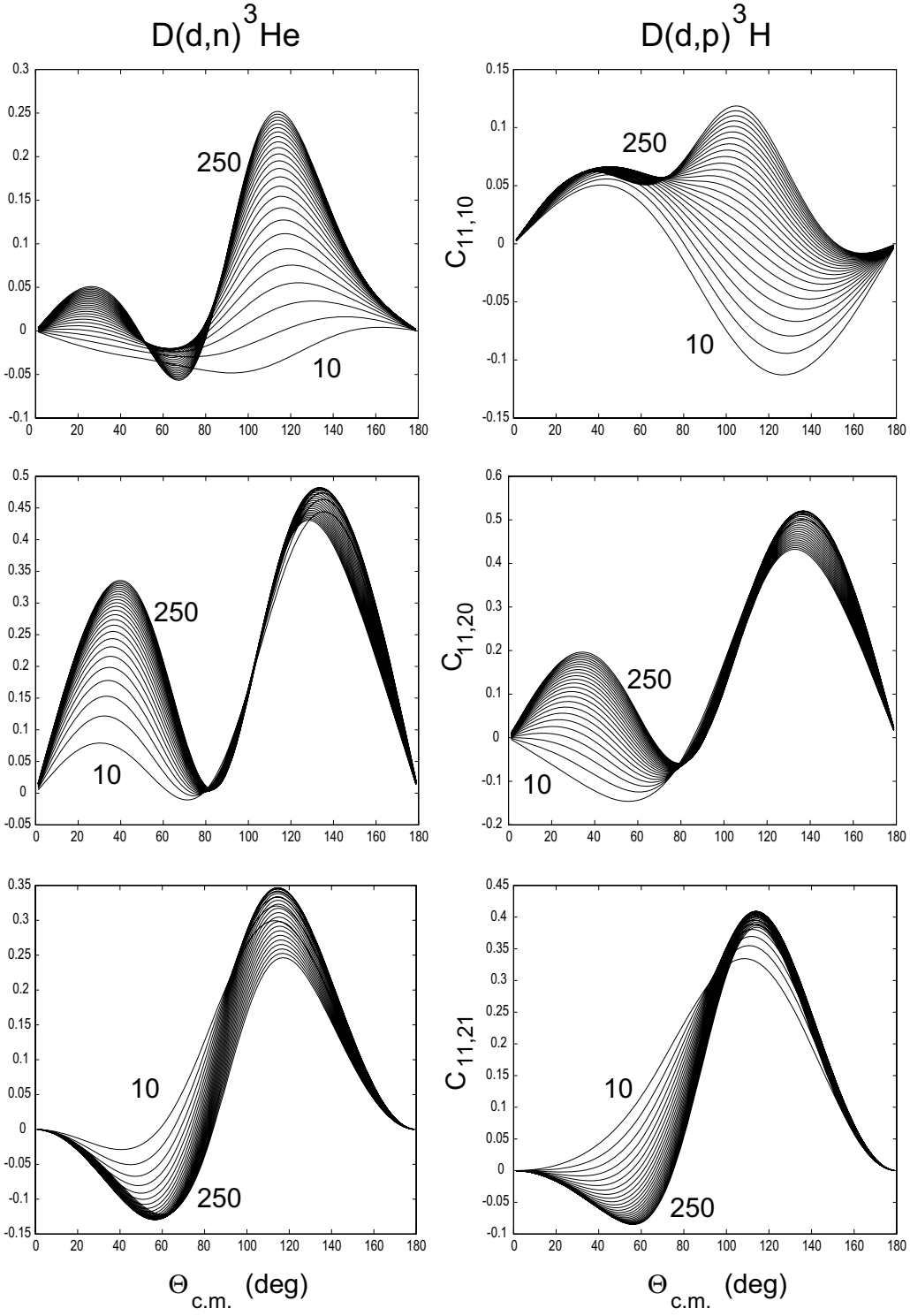

Fig. 41. The same as fig. 38.

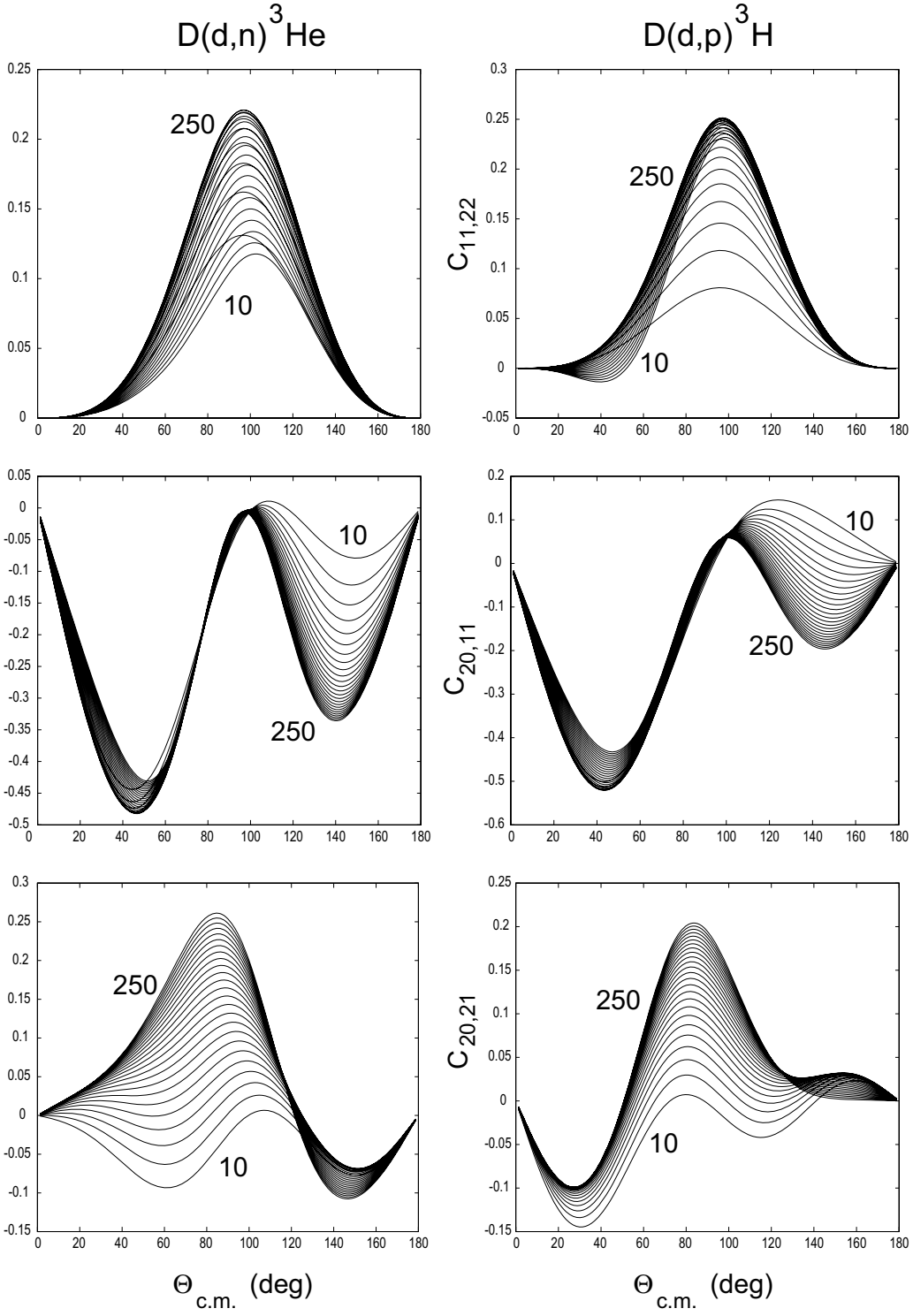

Fig. 42. The same as fig. 38.

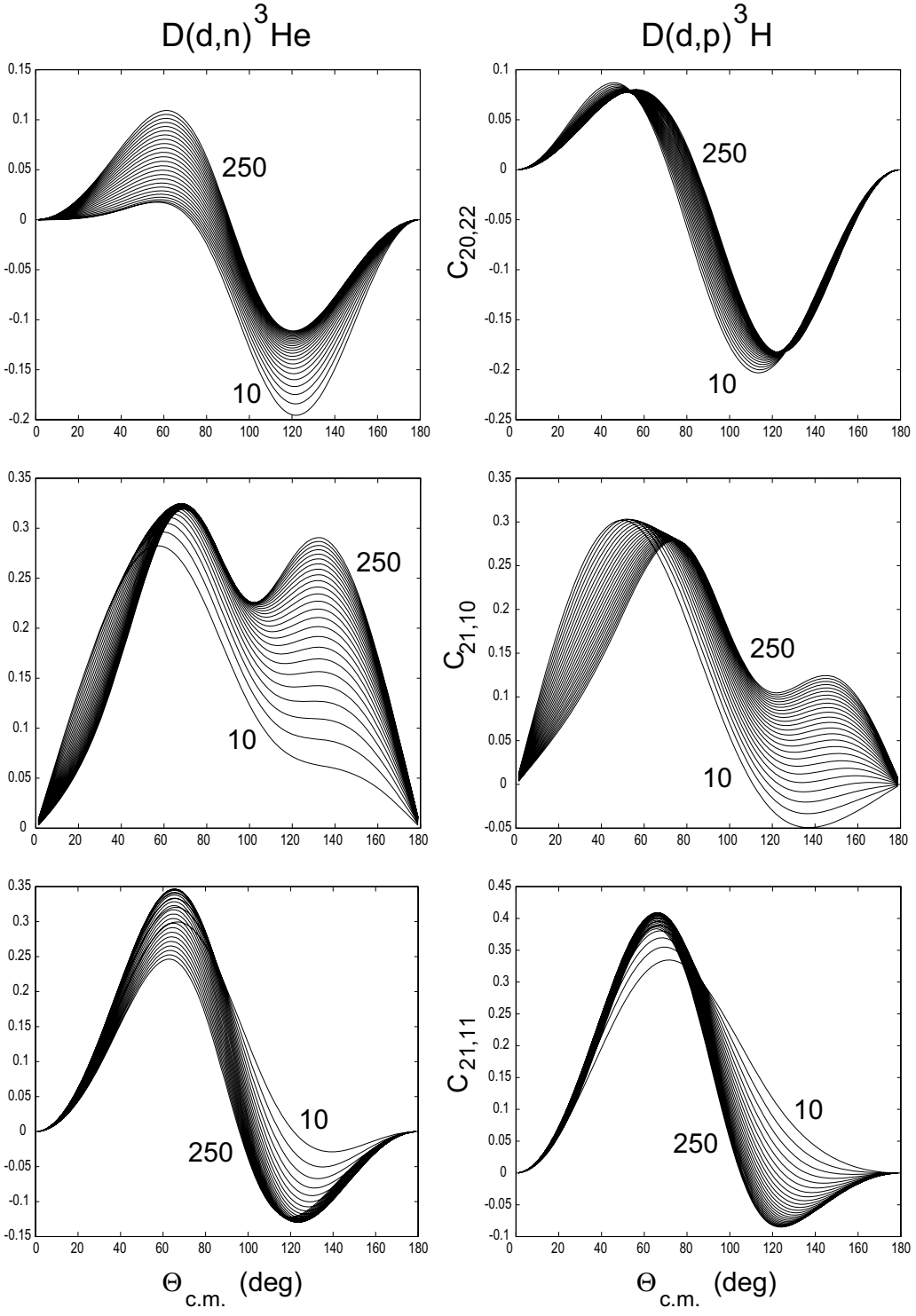

Fig. 43. The same as fig. 38.

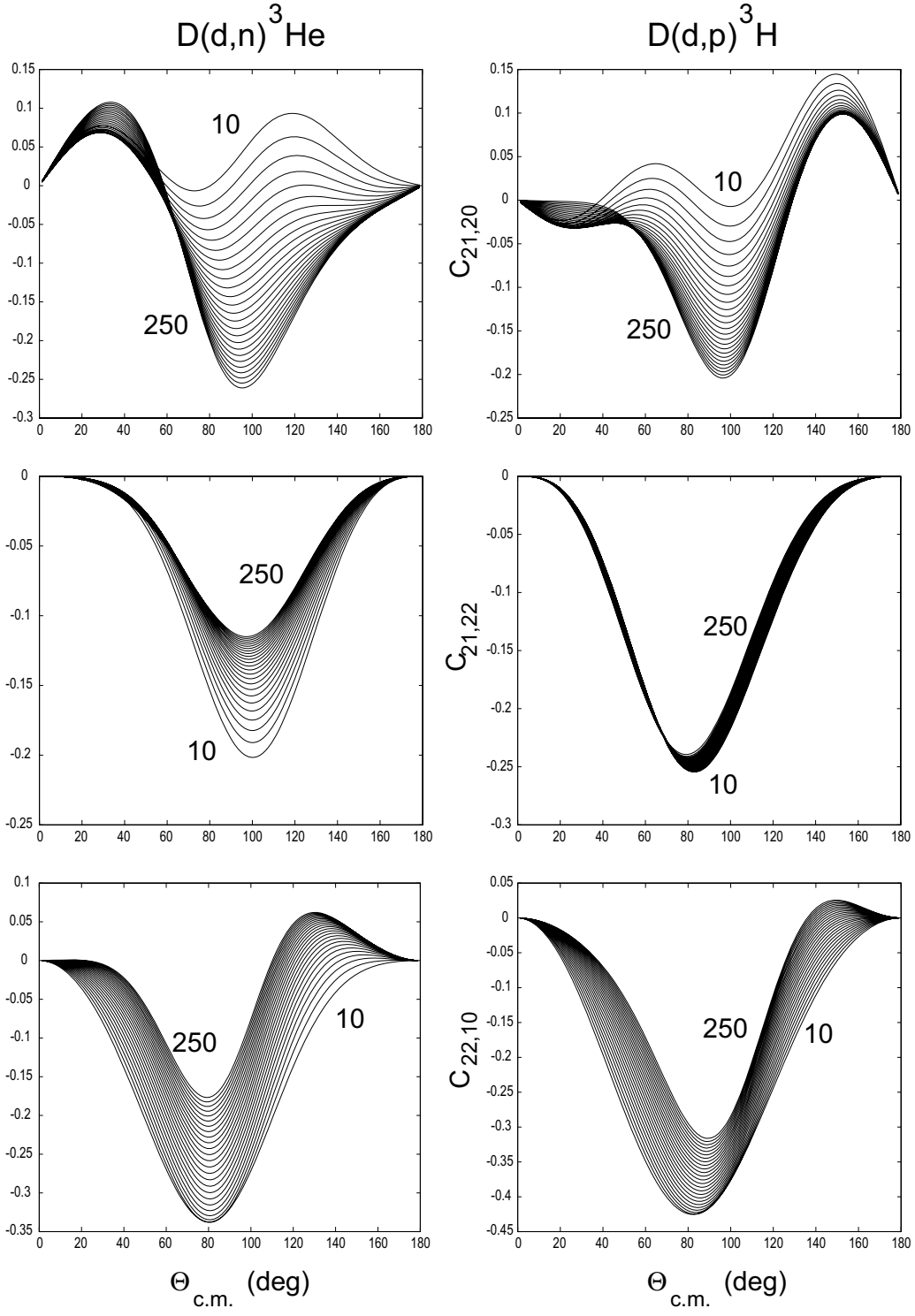

Fig. 44. The same as fig. 38.

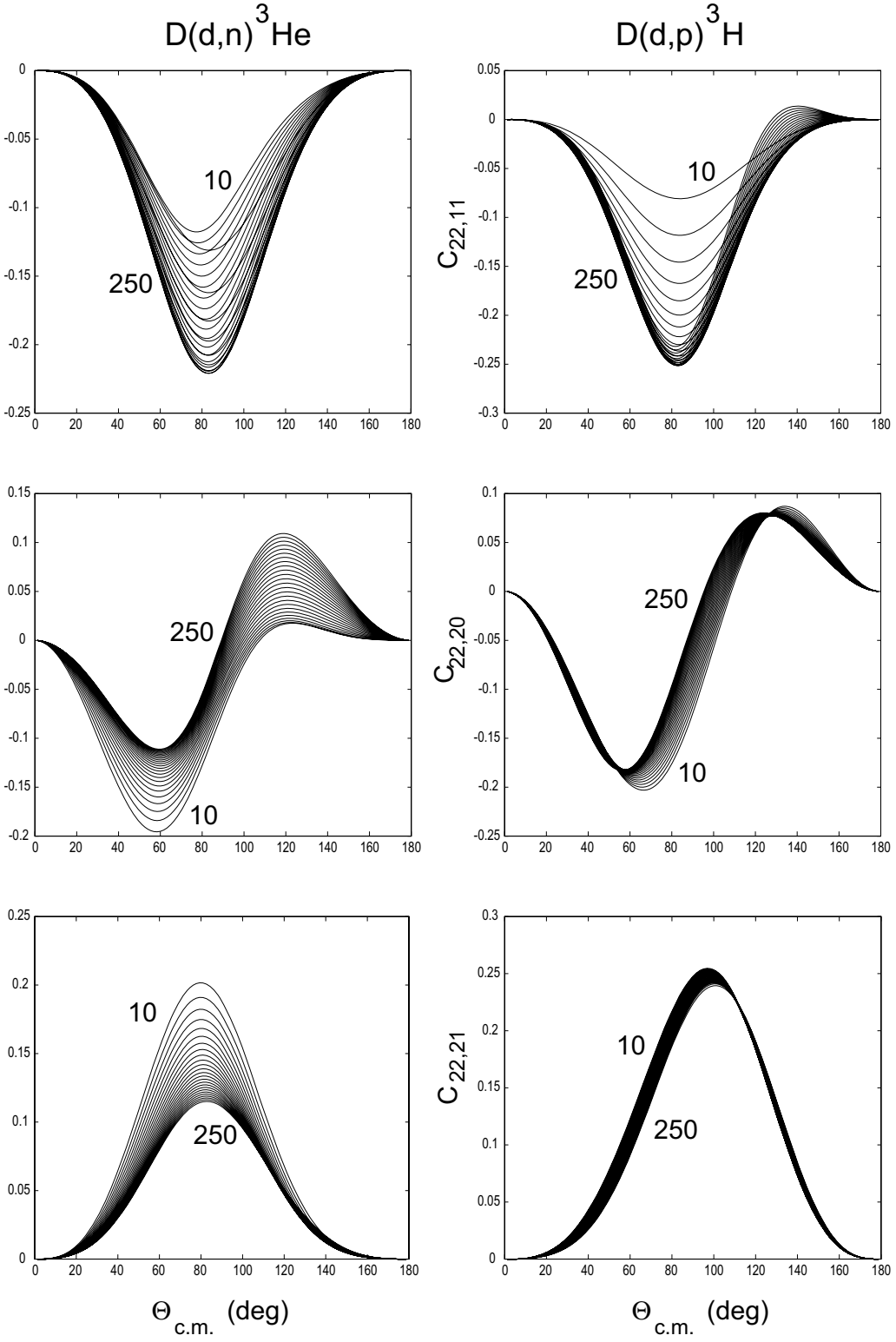

Fig. 45. The same as fig. 38.

Appendix B. Azimuthal dependence of polarized spin-1 on spin-1 cross-section

As mentioned in the text the observables (such as spin-correlation coefficients) depend only on the polar angle Θ, whereas the (polarized) cross-section generally acquires an azimuthal dependence via the introduction of coordinate systems. These are in principle arbitrary but we shall follow Ohlsen [11] and the Madison Convention [56]. In ref. [11] the case of the azimuthal dependence of spin-correlation cross-sections is explained for spin-1/2 on spin-1 systems (see also ref. [81]), but not for the spin-1 on spin-1 case.

In addition it is advisable to choose such a system that the description of a real experiment is as simple and intuitive as possible. In this repect the Cartesian description is more intuitive than the spherical one. The description of polarization components from polarized sources and polarized targets is best imagined in a space-fixed coordinate system in which the directions of the polarization vectors are described by two sets of polar and azimuthal angles (β_b, Φ_b) for the incident beam polarization and (β_t, Φ_t) for the target. The orientation of the tensor polarization is fixed to that of the polarization vector. As coordinate system here a set of axes x, y, and z is chosen, where z is identical with the incoming beam direction (along $\vec{k}_{in}$), y may be vertically upward, and x, y, and z form a right-handed screw.

On the other hand, we need a scattering-frame system where a Y-axis is defined by the direction of $\vec{k}_{in} \times \vec{k}_{out}$, the Z-axis coincides with z, and with the X-axis again forming a right-handed system together with $Z = z$. It is clear that this system is different for each detector, the position of which must be characterized by a polar angle Θ and some azimuthal angle. We demand that for the parts of the cross-section with only one particle type (beam or target) being polarized (leading to analyzing powers) we have the usual description of the azimuthal dependence on Φ (with a maximum azimuthal complexity of $\cos 2\Phi$). Figure 46 shows the relations between the polarization symmetry axes and the projectile helicity frame. The polarization components in the scattering frame are

$$
\begin{aligned}
p_X &= \hat{p}_Z \sin\beta_b \cos(\Phi_b - \Phi),\\
p_Y &= \hat{p}_Z \sin\beta_b \sin(\Phi_b - \Phi),\\
p_Z &= \hat{p}_Z \cos\beta_b,\\
p_{XY} &= \frac{3}{4}\hat{p}_{ZZ} \sin^2\beta_b \sin 2(\Phi_b - \Phi),\\
p_{YZ} &= \frac{3}{2}\hat{p}_{ZZ} \sin\beta_b \cos\beta_b \sin 2(\Phi_b - \Phi),\\
p_{XZ} &= \frac{3}{2}\hat{p}_{ZZ} \sin\beta_b \cos\beta_b \cos(\Phi_b - \Phi),\\
p_{XX} - p_{YY} &= \frac{3}{2}\hat{p}_{ZZ} \sin^2\beta_b \cos 2(\Phi_b - \Phi),\\
p_{ZZ} &= \frac{1}{2}\hat{p}_{ZZ}(3\cos^2\beta_b - 1),
\end{aligned}
$$

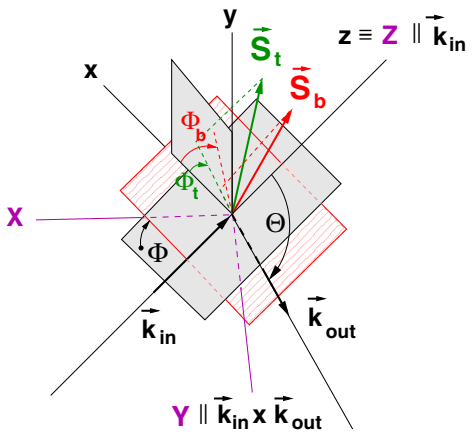

Fig. 46. Coordinate systems for spin-1 on spin-1 polarization correlation experiments. The polarization symmetry axes S_b for beam (b) and S_t for target (t) polarizations are defined in the space-fixed coordinate system x, y, and z. The detector(s) are positioned at polar angles Θ with respect to the $z = Z$ axis and at angles Φ as measured clockwise from the x-axis along z. Relative to the spin directions the azimuthal angles are $\Phi_b - \Phi$ and $\Phi_t - \Phi$.

and similarly for the target polarization

$$
\begin{aligned}
q_X &= \hat{q}_Z \sin\beta_t \cos(\Phi_t - \Phi),\\
q_Y &= \hat{q}_Z \sin\beta_t \sin(\Phi_t - \Phi),\\
q_Z &= \hat{q}_Z \cos\beta_t,\\
q_{XY} &= \frac{3}{4}\hat{q}_{ZZ} \sin^2\beta_t \sin 2(\Phi_t - \Phi),\\
q_{YZ} &= \frac{3}{2}\hat{q}_{ZZ} \sin\beta_t \cos\beta_t \sin 2(\Phi_t - \Phi),\\
q_{XZ} &= \frac{3}{2}\hat{q}_{ZZ} \sin\beta_t \cos\beta_b \cos(\Phi_t - \Phi),\\
q_{XX} - p_{YY} &= \frac{3}{2}\hat{p}_{ZZ} \sin^2\beta_t \cos 2(\Phi_t - \Phi),\\
q_{ZZ} &= \frac{1}{2}\hat{q}_{ZZ}(3\cos^2\beta_t - 1).
\end{aligned}
$$

The quantities $\hat{p}_i$, $\hat{p}_{jk}$, $\hat{q}_i$, $\hat{q}_{jk}$ are the (coordinate-system–independent) vector and tensor polarizations of beam and target as given by the occupation numbers of the hyperfine Zeeman states in a rotationally symmetric frame along the z-axis.

In the spin-correlation cross-section terms beam and target polarizations p and q appear as products. Therefore typical azimuthal dependences arise from combinations such as (and similarly for sin terms)

$$
\begin{aligned}
&\propto \cos(\Phi_b - \Phi) \cdot \cos(\Phi_t - \Phi),\\
&\propto \cos 2(\Phi_b - \Phi) \cdot \cos(\Phi_t - \Phi),\\
&\propto \cos 2(\Phi_b - \Phi) \cdot \cos 2(\Phi_t - \Phi).
\end{aligned}
$$

By using trigonometric relations it can be seen that these terms lead to azimuthal dependences $\propto [\cos M\Phi]_{M=0,1,\ldots}$ and therefore to a maximum

"complexity" of $\cos 4\Phi$ and also $\sin 4\Phi$, *e.g.*, for the correlation coefficient $C_{xy,xy}$. For this coefficient the product $\sin 2(\phi_b - \Phi) \cdot \sin 2(\Phi_t - \Phi)$ may be transformed into

$$\frac{1}{2}(\cos 4\Phi + 1) \sin 2\Phi_b \sin 2\Phi_t$$
$$-\frac{1}{2}(\cos 4\Phi - 1) \cos 2\Phi_b \cos 2\Phi_t$$
$$-\frac{1}{2} \sin 4\Phi (\cos 2\Phi_b \sin 2\Phi_t + \cos 2\Phi_t \sin 2\Phi_b).$$

This complexity has to be met by a sufficiently fine-grained detector arrangement. It is clear that substantial simplifications arise with the choice of special polarization directions. If, *e.g.*, in an experiment both polarization vectors point in the X-direction, then with $\Phi_b = \Phi_t = 0$ only a simple Φ-dependence $\propto (1 - \cos 4\Phi)$ of the cross-section results for this correlation coefficient. Of course the proper Φ-dependence has to be established for all coefficients.

References

1. R.M. Kulsrud, H.P. Furth, E.J. Valeo, M. Goldhaber, Phys. Rev. Lett. **49**, 1248 (1982).
2. R.M. Kulsrud, Nucl. Instrum. Methods A **271**, 4 (1988).
3. M. Tanaka (Editor), *Proceedings of the RCNP Workshop on Spin Polarized Nuclear Fusions (POLUSION99)* (RCNP, Osaka, 1999).
4. A. Honig, A. Sandorfi, *Proceedings of the 17th International Spin Physics Symposium (SPIN2006), Kyoto*, edited by K. Imai, T. Murakami, N. Saito, K. Tanida, AIP Conf. Proc. **915**, 1010 (2007).
5. A. Huke, K. Czerski, P. Heide, G. Ruprecht, N. Targosz, W. Żebrowski, Phys. Rev. C **78**, 015803 (2008).
6. Ch. Leemann, H. Bürgisser, P. Huber, U. Rohrer, H. Paetz gen. Schieck, F. Seiler, Helv. Phys. Acta **44**, 141 (1971).
7. Ch. Leemann, H. Bürgisser, P. Huber, U. Rohrer, H. Paetz gen. Schieck, F. Seiler, Ann. Phys. (N.Y.) **66**, 810 (1971).
8. W.H. Geist, C.R. Brune, H.J. Karwowski, E.J. Ludwig, K.D. Veal, G.M. Hale, Phys. Rev. C **60**, 054003 (1999).
9. Braizinha, C.R. Brune, A.M. Eiró, B.M. Fisher, H.J. Karwowski, D.S. Leonard, E.D. Ludwig, F.D. Santos, I.J. Thompson, Phys. Rev. C **69**, 0246008 (2004).
10. H. Grunder, R. Gleyvod, G. Lietz, G. Morgan, H. Rudin, F. Seiler, A. Stricker, Helv. Phys. Acta **44**, 662 (1971).
11. G.G. Ohlsen, Rep. Progr. Phys. **35**, 717 (1972).
12. M.P. Rekalo, E. Tomasi-Gustafsson, Phys. Rev. C **57**, 2870 (1998).
13. B. Becker, R. Randermann, B. Polke, S. Lemaître, R. Reckenfelderbäumer, P. Niessen, G. Rauprich, L. Sydow, H. Paetz gen. Schieck, Few-Body Syst. **13**, 19 (1992).
14. J. Raeder *et al.*, *Kontrollierte Kernfusion* (Teubner, Stuttgart, 1987).
15. F. Raiola *et al.*, Eur. Phys. J. A **13**, 377 (2002).
16. C. Rolfs, E. Somorjai, Nucl. Instrum. Methods: Phys. Res. B **99**, 297 (1995).
17. O.A. Yakubovsky, Sov. J. Nucl. Phys. **5**, 937 (1967).
18. H.M. Hofmann, in *Proceedings of Models and Methods in Few-Body Physics, Lisboa, Portugal, 1986*, edited by L.S. Ferreira, A.C. Fonseca, L. Streit, Lect. Notes Phys. **273**, 243 (1987).
19. J.A. Tjon, Phys. Lett. B **56**, 217 (1975).
20. E. Epelbaum, Phys. Lett. B **639**, 456 (2006).
21. E. Epelbaum, Prog. Part. Nucl. Phys. **57**, 654 (2006).
22. R.H. Cyburt, Phys. Rev. D **70**, 023505 (2004).
23. W. Glöckle, H. Witała, D. Hüber, H. Kamada, J. Golak, Phys. Rep. **274**, 107 (1996).
24. M. Viviani, A. Kievsky, L.E. Marcucci, S. Rosati, Nucl. Phys. A **751**, 226c (2005).
25. A. Deltuva, A.C. Fonseca, P.U. Sauer, Phys. Rev. C **72**, 054005 (2005).
26. E. Epelbaum, A. Nogga, W. Glöckle, H. Kamada, Ulf-G. Meißner, H. Witała, Phys. Rev. C **66**, 064001 (2002).
27. E. Epelbaum, Nucl. Phys. A **805**, 439c (2008).
28. W. Tornow *et al.*, J. Phys. G **35**, 125104 (2008).
29. H. Paetz gen. Schieck, Few-Body Syst. **30**, 81 (2001).
30. A. Fonseca, talk given at *INPC2007, Tokyo*.
31. H.M. Hofmann, G.M. Hale, Phys. Rev. C **77**, 044002 (2008).
32. M. Viviani, A. Kievsky, S. Rosati, E.A. George, K.L. Knutson, Phys. Rev. Lett. **86**, 3739 (2001).
33. A. Fonseca, *Proceedings of the International Conference on Nuclear Physics, Tokyo 2007*, Nucl. Phys. A **805**, 180c (2008).
34. E. Uzu, S. Oryu, M. Tanifuji, Prog. Theor. Phys. **90**, 937 (1993).
35. E. Uzu, S. Oryu, M. Tanifuji, in *POLUSION99* (RCNP, Osaka, 1999) p. 30.
36. A. Deltuva, private communication (2008).
37. A. Deltuva, A. Fonseca, Phys. Rev. C **76**, 021001(R) (2007).
38. Cl. Petitjean, P. Huber, H. Paetz gen. Schieck, H.R. Striebel, Helv. Phys. Acta **40**, 401 (1967).
39. H. Paetz gen. Schieck, P. Huber, Cl. Petitjean, H. Rudin, H.R. Striebel, Helv. Phys. Acta **40**, 414 (1967).
40. K. Jeltsch, P. Huber, A. Janett, H.R. Striebel, Helv. Phys. Acta **43**, 279 (1970).
41. E. Pfaff, PhD Thesis, Universität Gießen, unpublished, 1992.
42. Y. Tagishi, N. Nakamoto, K. Katoh, J. Togawa, T. Hisamune, T. Yoshida, Y. Aoki, Phys. Rev. C **46**, R1155 (1992).
43. K.A. Fletcher, Z. Ayer, T.C. Black, R.K. Das, H.J. Karwowski, E.J. Ludwig, G.M. Hale, Phys. Rev. C **49**, 2305 (1994).
44. H. Paetz gen. Schieck, Few-Body Syst. **5**, 171 (1988).
45. J.W. Gegner, Diploma Thesis, Universität Erlangen/Nürnberg, unpublished, 1989.
46. G.M. Hale, private communication (1991).
47. S. Lemaître, H. Paetz gen. Schieck, Few-Body Syst. **9**, 155 (1990).
48. G. Hale, G. Doolen, LA-9971-MS, Los Alamos (1984).
49. S. Lemaître, Diploma Thesis, Universität zu Köln, unpublished, 1989.
50. S. Lemaître, H. Paetz gen. Schieck, Ann. Phys. (Leipzig) **2**, 503 (1993).
51. O. Geiger, Diploma Thesis, Universität zu Köln, unpublished, 1993.
52. O. Geiger, S. Lemaître, H. Paetz gen. Schieck, Nucl. Phys. A **586**, 140 (1995).
53. T.A. Welton, in *Fast Neutron Physics II*, edited by J.B. Marion, J.L. Fowler (Interscience, New York, 1963) p. 1317.
54. F. Seiler, Comput. Phys. Commun. **6**, 229 (1974).
55. F. Seiler, E. Baumgartner, Nucl. Phys. A **153**, 193 (1970).

56. H. Barschall, W. Haeberli (Editors), *Proceedings of the Third International Symposium on Polarization Phenomena in Nuclear Reactions, Madison, 1970* (The University of Wisconsin Press, 1971) p. XXV.
57. P. Heiss, Z. Phys. **251**, 159 (1972).
58. K.P. Nyga, private communication, 1985.
59. H. Aulenkamp, Diploma Thesis, Universität zu Köln, unpublished, 1973.
60. B.P. Ad'yasevich, V.G. Antonenko, P. Bém, P. Kozma, J. Mareš, Czech. J. Phys. B **32**, 1349 (1982).
61. P. Kozma, P. Bém, B.P. Ad'yasevich, V.G. Antonenko, Czech. J. Phys. B **35**, 1118 (1985).
62. B.P. Ad'yasevich, D.E. Fomenko, Sov. J. Nucl. Phys. **9**, 167 (1969).
63. H.M. Hofmann, G.M. Hale, R. Wölker, *Proceedings of the International Workshop on Few-Body Approaches to Nuclear Reactions in Tandem and Cyclotron Energy Regions, Tokyo, 1986*, edited by S. Oryu, T. Sawada (World Scientific, Singapore, 1986) p. 162.
64. K.F. Liu, J.S. Zhang, G.W. Shuy, Phys. Rev. Lett. **55**, 1649 (1985).
65. J.S. Zhang, K.F. Liu, G.W. Shuy, Phys. Rev. Lett. **57**, 1410 (1986).
66. D. Fick, H.M. Hofmann, Phys. Rev. Lett. **55**, 1650 (1985).
67. H.M. Hofmann, D. Fick, Phys. Rev. Lett. **52**, 2038 (1984).
68. E. Uzu, nucl-th/0210026 (2002).
69. J.S. Zhang, K.F. Liu, G.W. Shuy, Phys. Rev. C **60**, 054614 (1999).
70. A. Deltuva, private communication (2009).
71. T. Katabuchi, K. Kudo, K. Masuno, T. Iizuka, Y. Aoki, Y. Tagishi, Phys. Rev. C **64**, 047601 (2001).
72. A. Imig, C. Düweke, R. Emmerich, J. Ley, K.O. Zell, H. Paetz gen. Schieck, Phys. Rev. C **73**, 024001 (2006).
73. D.S. Leonard, H.J. Karwowski, C.R. Brune, B. Fisher, E.J. Ludwig, Phys. Rev. C **73**, 045801 (2006).
74. A. Vassiliev, N. Chernov, K. Grigoriev, S. Sherman, R. Engels, F. Rathmann, H. Seyfarth, U. Uzikov, Czech. J. Phys. Suppl. **54**, C1 (2004).
75. R. Engels, private communication (2006).
76. R. Emmerich, H. Paetz gen. Schieck, Nucl. Instrum. Methods A **586**, 387 (2008).
77. V. Bechtold, L. Friedrich, P. Ziegler, R. Aniol, G. Latzel, H. Paetz gen. Schieck, Nucl. Instrum. Methods **150**, 407 (1978).
78. H. Brückmann, D. Finken, L. Friedrich, Nucl. Instrum. Methods **87**, 155 (1970).
79. L.D. Knutson, Phys. Rev. A **2**, 1878 (1970).
80. R. Engels, R. Emmerich, J. Ley, G. Tenckhoff, H. Paetz gen. Schieck, Rev. Sci. Instrum. **74**, 345 (2003).
81. B.v. Przewoski *et al.*, Phys. Rev. C **74**, 064003 (2006).